GEAP-4481
AEC Research
and Development Report
January 15, 1964

FUEL CYCLE PROGRAM

A BOILING WATER REACTOR
RESEARCH AND DEVELOPMENT PROGRAM

FOURTEENTH QUARTERLY PROGRESS REPORT

October - December 1963

Compiled by
C. L. Howard

U. S. ATOMIC ENERGY COMMISSION
CONTRACT AT(04-3)-189
PROJECT AGREEMENT 11

Printed in U. S. A. ~~Price $1.75~~. Available from the
Office of Technical Services, Department of Commerce,
Washington 25, D. C.

ATOMIC POWER EQUIPMENT DEPARTMENT
GENERAL ELECTRIC
SAN JOSE, CALIFORNIA

1661-T10-2
75 3/64

TABLE OF CONTENTS

LIST OF ILLUSTRATIONS

LIST OF TABLES

INTRODUCTION

The Fuel Cycle Program is an integrated program of investigation in the Vallecitos Boiling Water Reactor (VBWR) and other facilities to improve the technological limits of boiling water reactors in the following areas:

Task A

1. Extend fuel life information on oxide fuel at high specific power operation and raise the performance limits of oxide fuels.

2. Study power stability and performance characteristics of an oxide-fueled core under natural and forced circulation to improve design limits. (Terminated, see this report and GEAP-3971.)

Task B

Conduct out-of-pile experiments in heat transfer and fluid dynamics in the areas of burnout heat transfer, steam void observational studies, and two-phase pressure drop to support in-core work. (Terminated, see GEAP-4301 and 4383.)

Task C

Study long-term reactivity and isotopic composition changes for fuels having lattice characteristics of large power reactors. (Terminated, see GEAP-4107 and 4301.)

This report is written in partial fulfillment of contract AT(04-3)-189, Project Agreement No. 11, Fuel Cycle Program, between the United States Atomic Energy Commission and the General Electric Company. Prior reports to the Commission under this contract have included the following:

1. GEAP-3516, First Summary Progress Report, March 1959 - July 1960.
2. GEAP-3558, First Quarterly Progress Report, August - September 1960.
3. GEAP-3627, Second Quarterly Progress Report, October - December 1960.
4. GEAP-3628, Prediction of Two-Phase Flow From Mixing Length Theory, S. Levy, December 27, 1960. Revision I, May 31, 1961.
5. GEAP-3709, Third Quarterly Progress Report, January - March 1961.
6. GEAP-3655, Pressure Drop Along a Fuel Cycle Fuel Assembly, Various Orifice Configurations, E. Janssen and J. A. Kervinen, May 22, 1961.
7. GEAP-3781, Fourth Quarterly Progress Report, April - June 1961.
8. GEAP-3794, Plan for VBWR Stability Experiment, W. H. Cook, et al., August 30, 1961.
9. GEAP-3835, Fifth Quarterly Progress Report, July - September 1961.
10. GEAP-3898, Sixth Quarterly Progress Report, October - December 1961.
11. GEAP-3953, Seventh Quarterly Progress Report, January - March 1962.
12. GEAP-3766, Critical Heat Flux and Flow Pattern Characteristics of High Pressure Boiling Water in Forced Convection, F. E. Tippets, April 1962.

13. GEAP-3961, Prediction of the Critical Heat Flux in Forced Convection Flow, S. Levy, June 20, 1962.

14. GEAP-4048, Eighth Quarterly Progress Report, April - June 1962.

15. GEAP-4061, Water Surface Waves in Boiling Water Reactors, C. L. Howard and R. G. Hamilton, August 31, 1962.

16. GEAP-4094, Ninth Quarterly Progress Report, July - September 1962.

17. GEAP-4098, Evaluation of Zirconium 1.5 W/O Niobium Cladding for Use in Boiling Water Environments, C. J. Baroch and W. C. Rous, October 1962.

18. GEAP-4107, Heavy Element Isotopic Analysis of UO_2 Fuel Irradiated in the VBWR, Report No. 1, M. R. Hackney and C. P. Ruiz, December 1962.

19. GEAP-4159, Tenth Quarterly Progress Report, October - December 1962.

20. GEAP-3899, Burnout Conditions for Single Rod in Annular Geometry, Water at 600 to 1400 psia, E. Janssen and J. A. Kervinen, February 1963.

21. GEAP-4203, Methods for Improving the Critical Heat Flux of BWR's, C. L. Howard, March 1963.

22. GEAP-3653, AEC Fuel Cycle Program, Design and Fabrication of the Basic Fuel Assemblies, C. J. Baroch, J. P. Hoffmann and W. C. Rous, March 1963.

23. GEAP-4206, Evaluation of the Failed BMI Hot Gas Isostatic Pressed Fuel Rods, C. J. Baroch, C. B. Boyer and S. W. Porembka, March 1963.

24. GEAP-4215, Eleventh Quarterly Progress Report, January - March, 1963.

25. GEAP-4257, Design and Fabrication of Fuel Rods Containing Low Temperature Sintered Pellets, C. J. Baroch, May 15, 1963.

26. GEAP-4282, Design and Fabrication of Coextruded Stainless Steel Clad - UO_2 Fuel Rods. C. J. Baroch, June, 1963.

27. GEAP-3755, Burnout Conditions for Nonuniformly Heated Rod in Annular Geometry, Water at 1000 psia, E. Janssen and J. A. Kervinen, June, 1963.

28. GEAP-4301, Twelfth Quarterly Progress Report, July - September, 1963.

29. GEAP-4312, Design and Fabrication of Special Assembly 12-L, Two Designs for Utilizing Boron as Burnable Poison, S. Y. Ogawa and H. E. Williamson, July 15, 1963.

30. GEAP-4394, Design and Fabrication of Special Assembly 10L, Compacted Powder Fuel Rods Clad with 0.127 mm Wall Stainless Steel, S. Y. Ogawa and H. E. Williamson, September, 1963.

31. GEAP-4358, Critical Heat Flux for Multirod Geometry, J. E. Hench, September, 1963.

32. GEAP-4383, Thirteenth Quarterly Progress Report, July - September, 1963

33. GEAP-4408, A Uranium Dioxide Fuel Rod Center Melting Test in the Vallecitos Boiling Water Reactor, H. E. Williamson and J. P. Hoffmann, November, 1963

34. GEAP-3971, VBWR Stability Test Report, by members of Engineering Development, June 1963, (Released January 1964).

SUMMARY

1. Operation of the VBWR was terminated December 9, 1963, and all the fuel has been unloaded.

2. Fuel irradiations in the VBWR have resulted in exposure increases of 1100 to 1200 MWD/T (average) for the lead assemblies of each type. The terminal exposure status is as follows:

Fuel Designation and Clad	Number of Assemblies Under Test	Burnup, MWD/T Average of Group	Burnup, MWD/T Average for Lead Assembly
H - Annealed stainless steel (Control rod follower)	10	7400	8599
I - Cold worked stainless	16	6780	9193
J - Zircaloy	24	6250	9643
L - Special	11	--	7327

3. Examination of the basic fuel has revealed the following failures:

Fuel	Exposure, MWD/T	Sipping Signal	Visual
Annealed stainless steel			
9H	8599	yes	Circumferential cracks; Figure 3.
8H	7770	yes	Circumferential cracks - piece of rod missing: Figure 2.
4H (2 rods)	8485	yes	Circumferential cracks; Figure 1.
Cold-worked stainless steel			
9I	8252	yes	Long Longitudinal crack; Figure 4.
1I	7044	yes	Small crack
8I	9193	yes	Not inspected
16I	8042	yes	Not inspected
Zircaloy			
Zr-2 14J	8358	yes	Wear through clad at spacer.
Zr-4 25J	5774	yes	Conical hole; Figure 5.

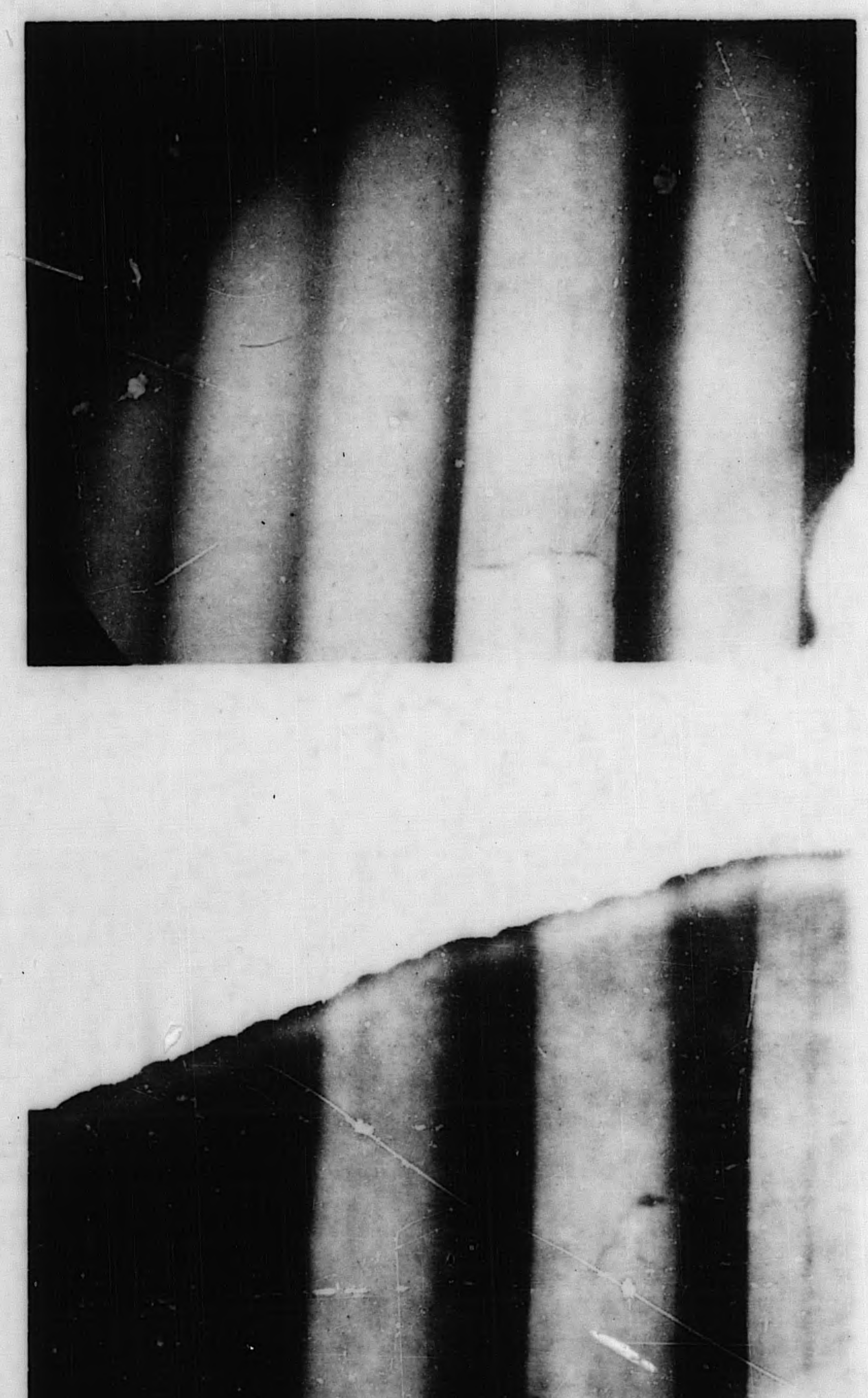

Figure 1. Failed Fuel Rods in Assembly 4H

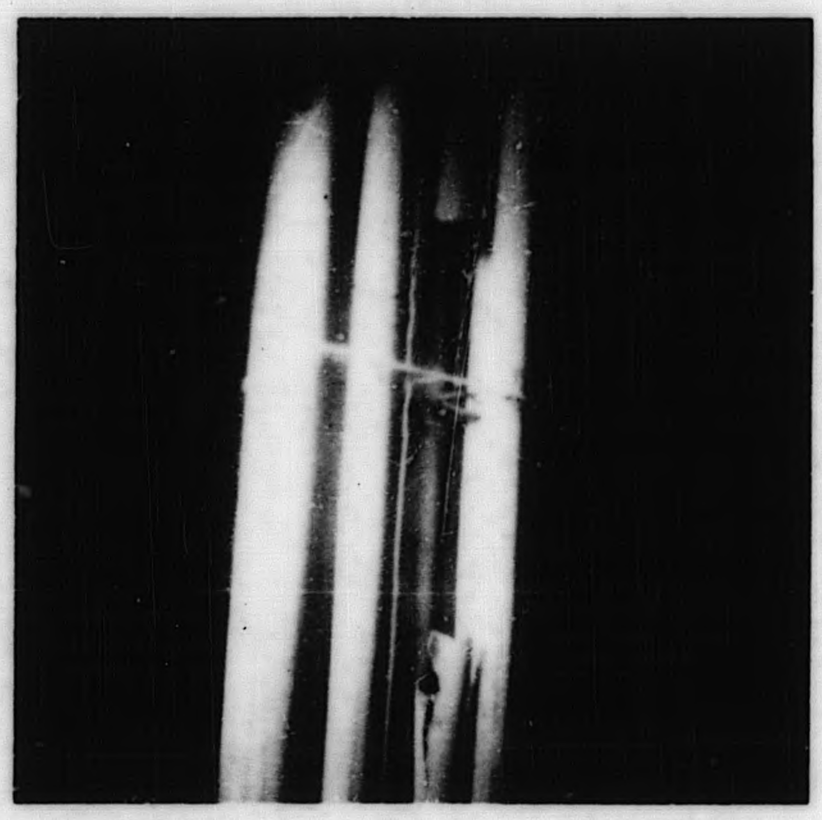

Figure 2. Failed Fuel Rod in Assembly 8H

Figure 3. Failed Fuel Rod in Assembly 9H

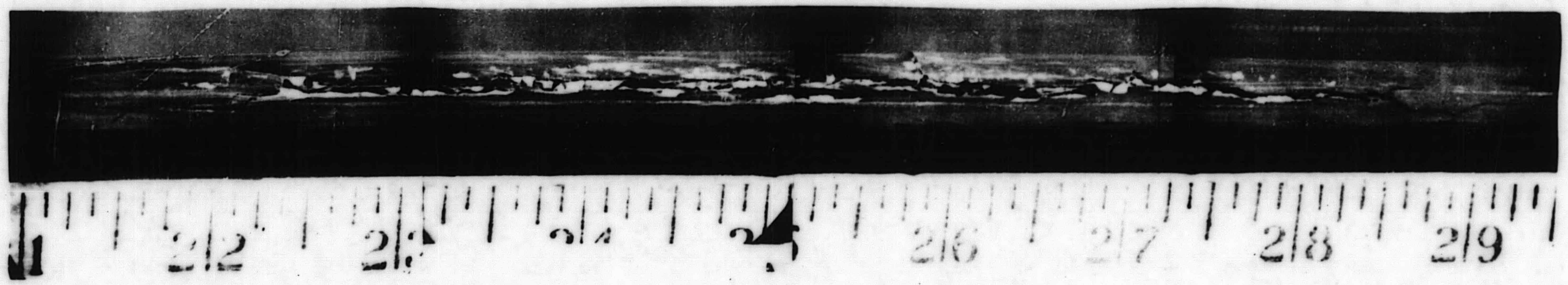

Figure 4. Failed Fuel Rod in Assembly 91

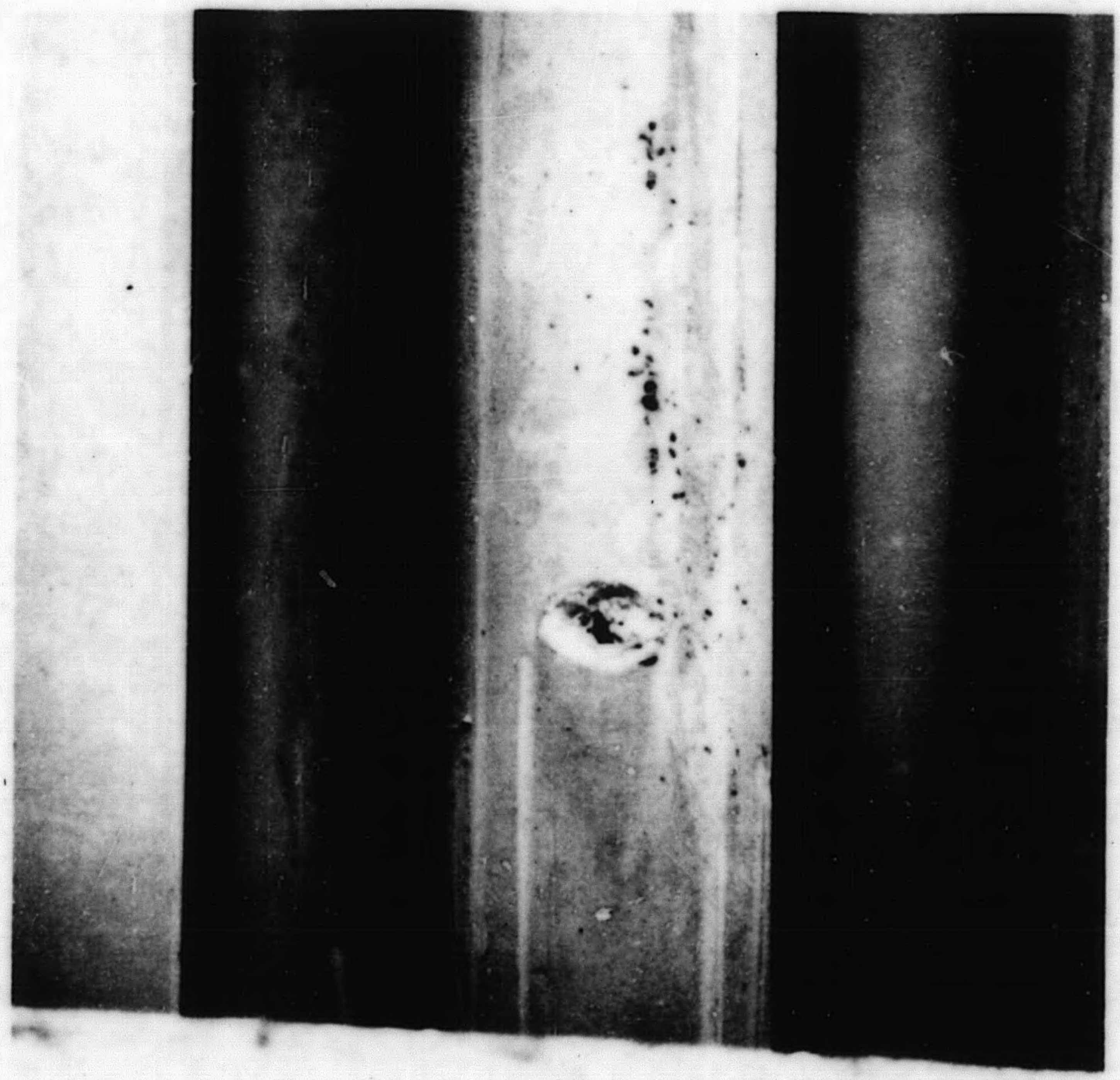

Figure 5. Failure in Assembly 25J

4. Fretting wear observations for Zircaloy clad with different spacer designs include:

Assembly	Spacer	Results
14J	Single-layer wire	Worn through clad, apparently prior to installing spring clips in the fall of 1962.
12J, 13J	Double-layer wire	Slight wear.
11J, 25J	Constant pressure springs	No wear - absence of crud at contact points.

5. A plot of percent of fuel rods failed versus average burnup for the group (Figure 6) shows that the annealed stainless steel clad H assemblies and cold-worked stainless steel I assemblies both have the same failure expectancy as the cold-worked E and F assemblies of the High Power Density (HPD) program.

6. Preliminary examination results for special fuel are as follows:

   a. A Zr-4 clad corner rod in assembly 6L has a circumferential crack in the weld zone at the lower end plug (Figure 7).

   b. All five 8L pellet fuel rods clad with 0.005-inch annealed stainless steel have wrinkles which run the entire length of the rod (Figure 8).

   c. The 10L compacted power fuel clad with 0.005-inch stainless steel has been pinched and wrinkled in the area just below the plenum support tube (Figure 9), presumably the result of UO_2 densification.

7. Detailed planning and scheduling for terminal RML examinations of each fuel type are in progress.

8. A topical report, "A uranium Dioxide Fuel Rod Center Melting Test in the Vallecitos Boiling Water Reactor," GEAP-4408, has been issued.

9. A terminal topical report on the stability task has been completed: "VBWR Stability Test Report," GEAP-3971. The stability work has been summarized as a conclusion to the task.

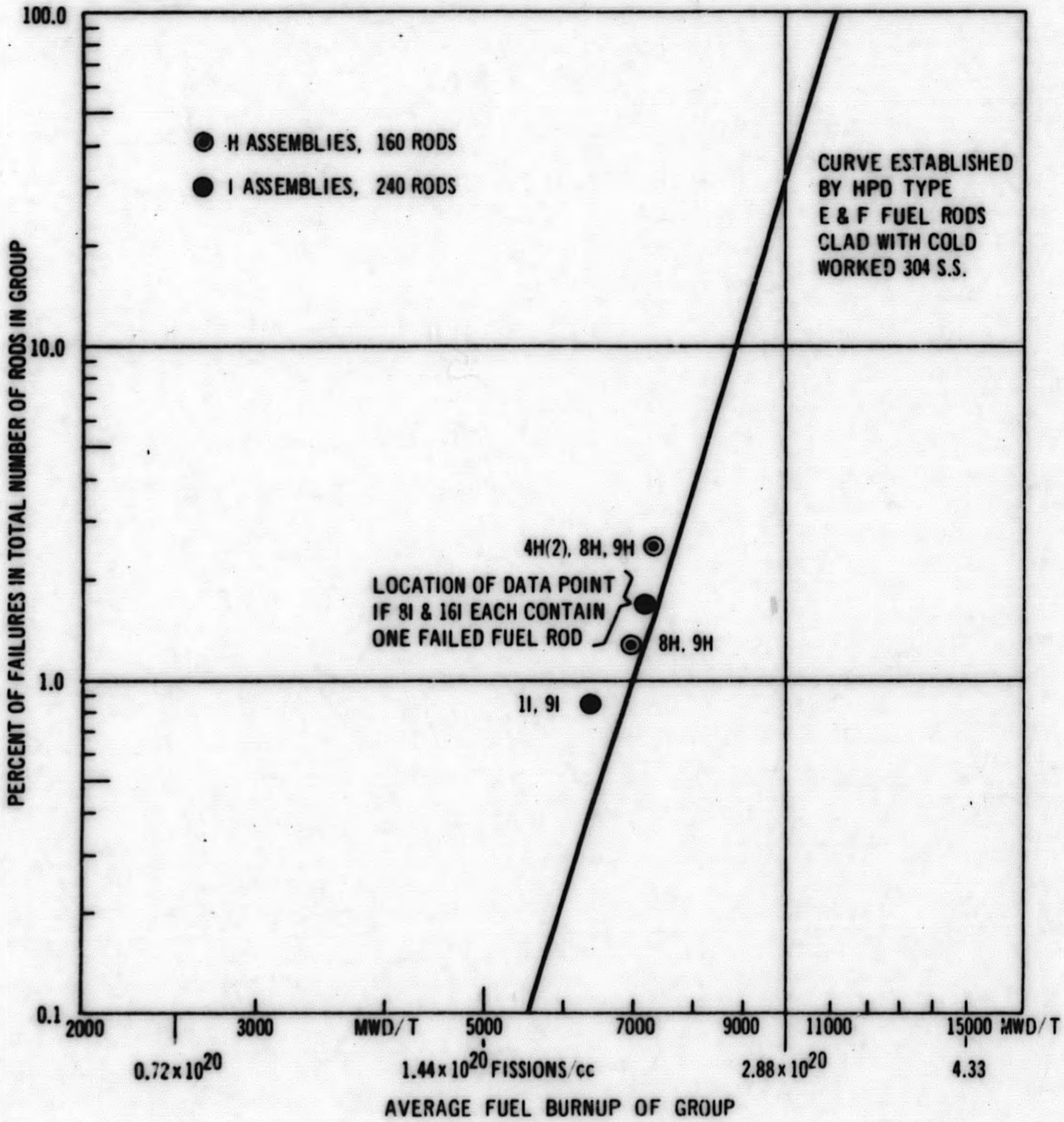

Figure 6. Percent Failure Versus Fuel Burnup for Failed Stainless Steel Clad Fuel Rods

Figure 7. Crack at Bottom End Plug Weld of Corner Rod C-4 of Assembly 6L

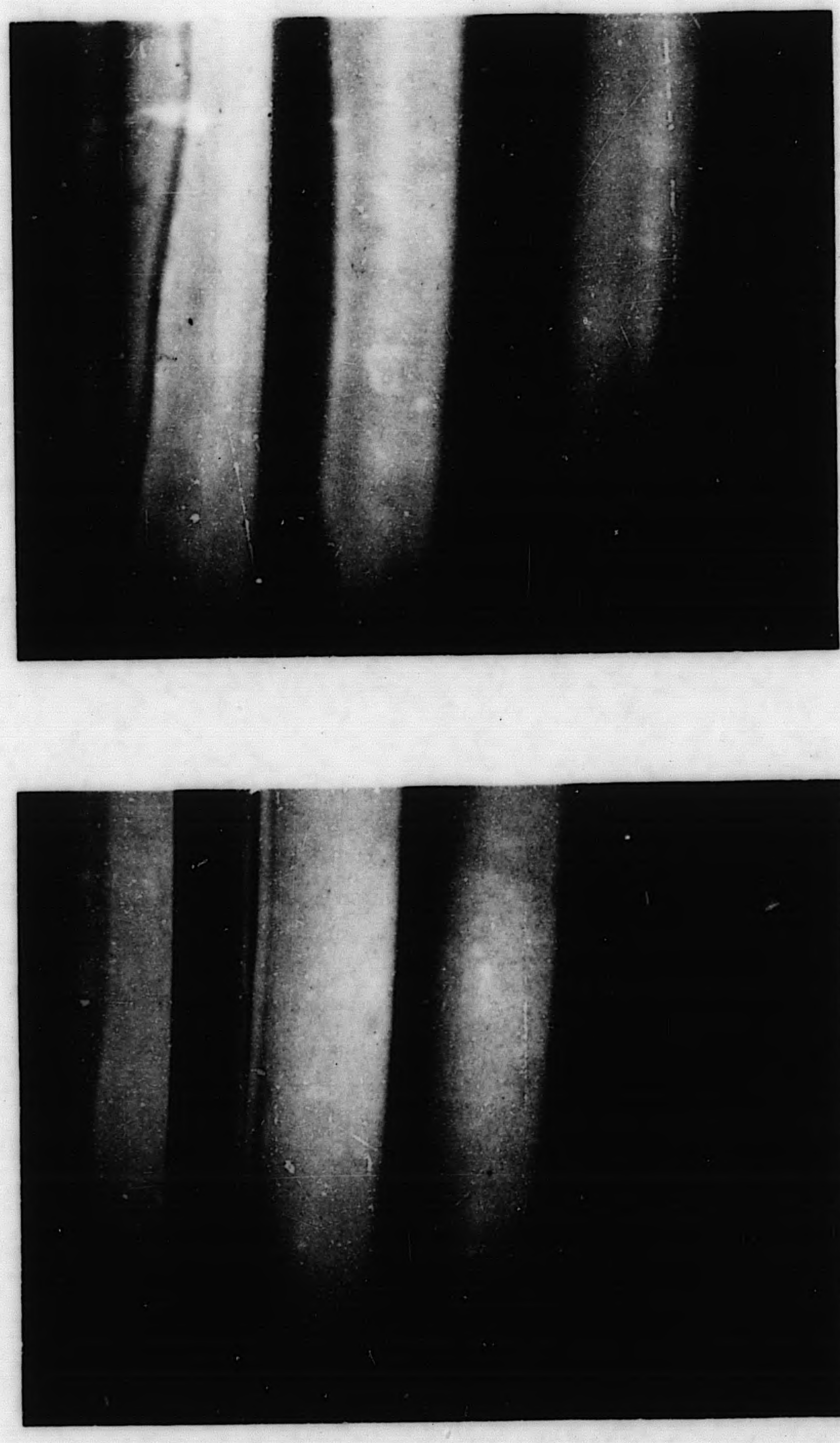

Figure 8. Wrinkled Fuel Rods in Assembly 8L

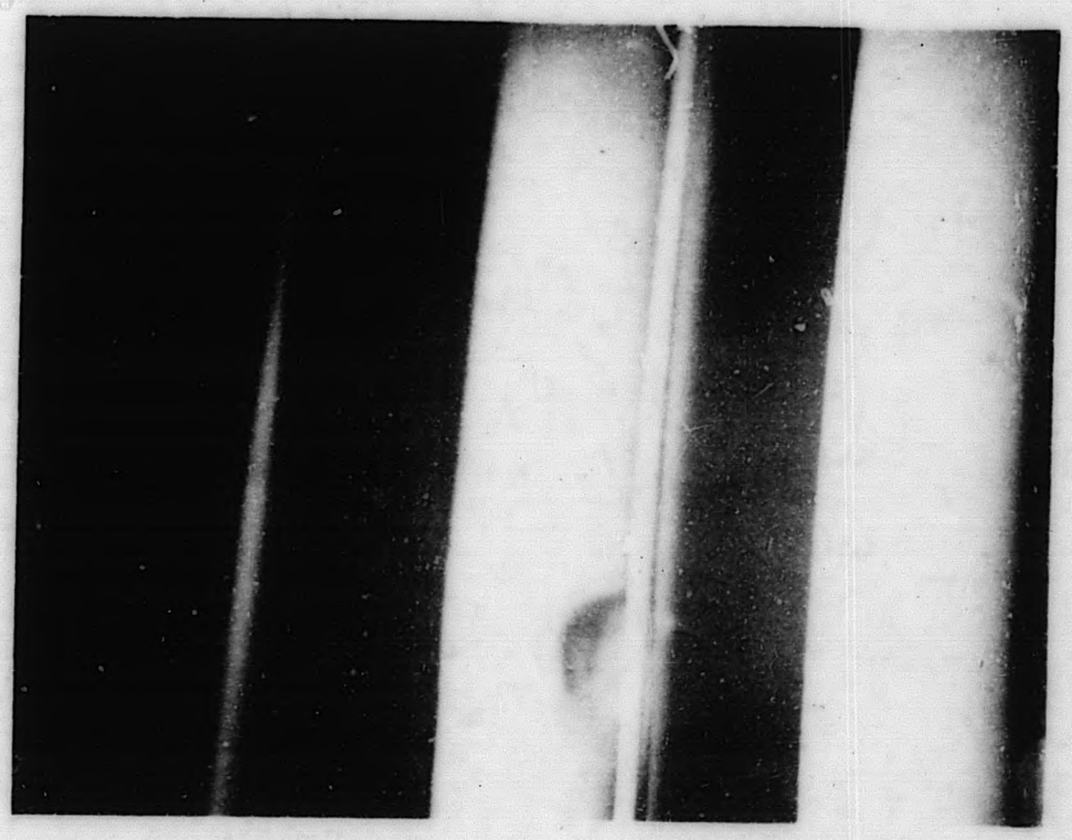

Figure 9. Pinched Clad at Top of Fuel Column in Assembly 10L

TASK A - ADVANCED FUEL POWER-LIMIT TESTS

A. Irradiation in the VBWR

This task provides for irradiation of the basic and special fuel assemblies. Irradiation of these assemblies in the VBWR was terminated on December 9, 1963, as reactor operation was discontinued by mutual agreement between the AEC and APED. Failed and selected non-failed fuel rods from both the basic and special fuel assemblies will be examined in detail.

B. Basic Fuel Program

The basic fuel program includes the irradiation and examination of a large number of stainless steel and Zircaloy clad fuel assemblies operated at high specific power in a boiling water reactor. The design and fabrication characteristics of the basic fuel are presented in Table I. Operational data to the time of the VBWR shutdown are presented in Table II and summarized below.

		Burnup,[1] Fissions/cc (MWD/T)	
Designation and Clad	Number	Average of Group	Average of Lead Assembly[2]
H - Annealed stainless steel (control rod follower)	10	2.13×10^{20} (7400)	2.48×10^{20} (8599)
I - Cold-worked stainless steel	16	1.92×10^{20} (6780)	2.65×10^{20} (9193)
J - Zircaloy	24	1.80×10^{20} (6250)	2.78×10^{20} (9643)

(1) Burnup as of VBWR Run 166 which was completed on December 9, 1963.

(2) Peak exposure is about 1.65 times this value.

1. Fuel Sipping and Pool Inspection

During the outage following Run 163 (October 6), sipping tests were performed to locate defective fuel elements. The sipping tests indicated that Assembly 9I contained a failed fuel rod. Visual examination in the VBWR pool revealed that the Assembly contained a failed corner rod.

Sipping tests conducted after Run 164 (October 21) indicated that Assemblies 1I, 8H, 9H, and 14J contained defective fuel rods. Visual examination of these assemblies in the VBWR pool confirmed that assemblies 1I, 8H, and 9H contained failed fuel rods. Detailed visual examination of Assembly 14J in the VBWR pool failed to reveal any defect. In-core sampling of the coolant from assembly 14J has indicated slight activity release since May, 1962.

TABLE I

DESIGN AND FABRICATION CHARACTERISTICS OF BASIC FUEL

Element Designation	Number of Rods	Clad Material	Room Temperature Yield Strength ($\times 10^{-3}$ kg/cm^2)	Wall Thickness (cm)	Tube OD (cm)	UO_2 Density Percent T. D.	UO_2 Enrichment Percent	Fabrication Process	UO_2 to Cold Clad Diametral Gap (cm)
1H	16	Type 304 stainless steel	2.81	0.051	1.07	94-96	2.76	S&GP (1)	0.008-0.020
2H									
3H									
4H									
5H									
6H									
7H									
8H									
9H									
10H	16	Type 304 stainless steel	2.81	0.051	1.07	94-96	2.76	S&GP	0.008-0.020
1I	16	Type 304 stainless steel	5.27	0.038	1.04	94-96	3.22	S& GP	0.002-0.022
2I									
3I	15								0.008-0.020
4I	16								
5I									
6I									
7I									
8I									
9I									
10I									
11I	16								
12I	16								
13I									
14I									
15I	14								
16I	16	Type 304 stainless steel	5.27	0.038	1.04	94-96	3.22	S&GP	0.008-0.020
1J	16	Zr-2	3.16	0.056	1.08	94-96	2.76	S&GP	0.008-0.020
2J									
3J									
4J									
5J									
6J									
7J									
8J							3.20		
9J							3.20		
10J							2.98		
11J							3.49		
12J	16	Zr-2	3.16	0.056	1.08	94-96	3.49	S&GP	0.008-0.020

TABLE I (Continued)

Element Designation	Number of Rods	Clad Material	Room Temperature Yield Strength ($\times 10^{-3}$ kg/cm^2)	Wall Thickness (cm)	Tube OD (cm)	UO_2 Density Percent T. D.	UO_2 Enrichment Percent	Fabrication Process	UO_2 to Cold Clad Diametral Gap (cm)
13J	16	Zr-2	3.16	0.056	1.08	94-96	3.49	S&GP	0.008-0.020
14J									
15J							2.98/3.49		
16J							2.76		
17J									
18J									
19J							2.76/2.98		
20J							2.98		
21J	14						2.98		
22J	14						3.49		
23J	16	Zr-2/Zr-4					2.76		
25J	16	Zr-2/Zr-4	3.16	0.056	1.08	94-96	2.76	S&GP	0.008-0.020

(1) Sintered and ground pellets

TABLE II

OPERATIONAL DATA OF BASIC FUEL

Element Designation	Peak Surface Heat Flux W/cm^2	Peak Surface Heat Flux Btu/hr ft^2 × 10^{-3}	Peak Fuel Center Temperature °C	Burnup Fissions/cc × 10^{-20}	Burnup MWD/T	Hours at Temperature (>5 MW)	Power Cycles 0 to >20 MW Back to 0	Thermal Cycles 0 to 75 MW Back to 0	Comments
1H	101	322	1,343	1.78	6,197	10,225	200	387	
2H	93	295	1,316	1.74	6,043	10,225	200	387	
3H	88	278	1,288	1.96	6,790	9,946	197	384	
4H	121	385	1,649	2.44	8,485	9,946	197	384	Failed Fuel rods (two)
5H	109	347	1,427	2.24	7,761	10,225	200	387	
6H	105	334	1,371	2.07	7,177	10,225	200	387	
7H	105	334	1,371	2.20	7,638	10,225	200	387	
8H	118	374	1,593	2.24	7,770	9,544	196	383	Failed Fuel rod
9H	127	402	1,815	2.48	8,599	9,544	196	383	Failed Fuel rod
10H	109	347	1,427	2.14	7,414	10,225	200	387	
1I	128	407	1,855	2.03	7,044	7,839	152	332	Failed Fuel rod
2I	111	352	1,427	1.93	6,698	8,737	161	290	
3I	114	362	1,538	1.98	6,863	10,225	200	387	
4I	125	398	1,815	2.13	7,386	10,225	200	387	
5I	113	358	1,482	1.67	5,788	10,225	200	387	
6I	113	360	1,510	1.63	5,652	8,496	185	367	
7I	126	400	1,815	1.75	6,074	9,176	167	303	
8I	133	422	1,927	2.65	9,183	10,225	200	387	Weak sipping signal
9I	132	419	1,900	2.38	8,252	9,390	195	382	Failed Fuel rod
10I	98	309	1,343	1.87	6,488	10,225	200	387	
11I	122	386	1,649	1.57	5,435	7,524	173	355	
12I	123	390	1,733	1.88	6,524	10,225	200	387	
13I	127	402	1,815	2.00	6,958	9,022	166	302	
14I	129	411	1,870	1.92	6,667	10,225	200	387	
15I	78	247	1,093	1.03	3,573	6,428	115	156	
16I	127	403	1,815	2.32	8,042	10,071	199	386	Weak sipping signal

TABLE II (Continued)

Element Designation	Peak Surface Heat Flux W/cm^2	Peak Surface Heat Flux Btu/hr ft^2 × 10^{-3}	Peak Fuel Center Temperature °C	Burnup Fissions/cc × 10^{-20}	Burnup MWD/T	Hours at Temperature (>5 MW)	Power Cycles 0 to >20 MW Back to 0	Thermal Cycles 0 to >5 MW Back to 0	Comments
1J	92	291	1,316	1.62	5,613	8,346	179	300	
2J	79	252	1,204	1.35	4,672	8,346	179	300	
3J	75	239	1,149	1.35	4,672	8,346	179	300	
4J	95	300	1,371	1.66	5,765	8,346	179	300	
5J	99	315	1,399	1.88	6,541	8,346	179	300	
6J	133	423	1,983	2.29	7,953	8,346	179	300	
7J	95	300	1,371	1.68	5,827	8,346	179	300	
8J	105	334	1,482	1.58	5,485	7,618	164	280	
9J	109	345	1,538	2.10	7,284	8,346	179	300	
10J	157	499	2,370	1.58	5,495	8,040	157	250	
11J	145	460	2,177	2.78	9,643	8,828	170	273	
12J	151	479	2,343	2.71	9,418	8,828	170	273	
13J	139	442	2,065	2.68	9,304	8,828	170	273	
14J	130	412	1,870	2.41	8,358	8,828	170	273	Slight leaker
15J	107	340	1,510	1.64	5,677	8,040	157	250	
16J	127	386	1,792	1.96	6,801	8,040	157	250	
17J	110	350	1,538	1.58	5,483	7,169	137	192	
18J	122	388	1,792	1.62	5,626	6,751	127	178	
19J	156	494	2,370	1.49	5,169	7,608	143	205	
20J	160	509	2,400	1.42	4,949	8,042	157	250	
21J	155	491	2,370	1.39	4,813	6,425	115	156	
22J	148	470	2,205	1.53	5,304	6,762	122	167	
23J	90	286	1,316	1.28	4,449	6,555	118	153	
25J	155	492	2,370	1.66	5,774	6,358	94	177	Failed Fuel rod

Sipping tests conducted after Run 165 (November 16) indicated Assembly 4H contained defective fuel rods. Visual examination in the VBWR pool revealed two cracked fuel rods. The other fuel follower, Assembly 3H, on the same control rod drive as Assembly 4H was replaced at the same time to preclude a repetition of the repair in the immediate future.

Sipping tests conducted following Run 166 (December 9) indicated that Assemblies 8I, 16I, 14J, and 25J may contain failed fuel rods. Examination of Assembly 25J in the VBWR pool indicated that at least one fuel rod contained a defect. Visual examinations of Assemblies 8I, 16I, and 14J are scheduled.

In addition to the sipping tests and examinations of the assemblies to locate failed fuel rods, the following inspections were performed in the VBWR pool:

a. Two rods removed from Assembly 11J and two rods removed from Assembly 12J were visually examined in the VBWR pool. Both of these assemblies contain double layer wire spacers. No abnormal conditions were observed on any of the rods. Intensive visual examination of the fuel rods at the spacer contact points did not reveal appreciable wear, but clad polishing was apparent at the contact points.

b. Several Zircaloy clad fuel assemblies were examined to determine whether spring clips installed to tighten the fuel rods in the top tie plate had arrested the fretting wear previously observed.[1] No new or propagating wear marks were located, thus indicating that the spring clips had considerably reduced the wear.

c. The 12 outside rods of both Assemblies 8I and 16I were ultrasonically inspected at the VBWR pool following VBWR Run 165 to determine whether any incipient failures were present in the fuel rods. The 8I assembly has the highest burnup of any of the assemblies clad with cold-worked stainless steel. The ultrasonic inspection revealed that there were several locations where defects of about 20 percent of the clad thickness were present. In an attempt to determine the rate of propagation of these cracks, the assemblies were returned to the VBWR for continued irradiation.

2. <u>Details of Fuel Rod Failures</u>

<u>Type H Cladding</u>

The failures in the Type H fuel rods (clad with 0.051 cm of annealed stainless steel) were predominately circumferential cracks occurring near the middle wire spacer. All of the failures which have been observed were present in the exterior rods. These rods have a burnup equal to or greater than the bundle average. The H assemblies (control rod followers) have variable axial positions in the core during reactor operation but at normal operating power are usually positioned such that the middle of the assembly coincides approximately with the peak flux. Consequently, it is probable that the failures in the Type H fuel rods occurred at the peak heat flux location.

Photographs of the failures observed in Assemblies 4H, 8H, and 9H are shown in Figures 1, 2, and 3. These failures are similar in appearance to those observed in the fuel rods clad with annealed stainless steel which failed from intergranular attack in the HPD Program.[(2)] The design characteristics and operational data of the failed H assemblies have been extracted from Tables I and II and are summarized in Table III.

Type I Cladding

Two fuel rods from Type I assemblies, clad with cold-worked stainless steel, have been visually confirmed as being failed, and sipping results indicate that Assemblies 8I and 16I may contain failed fuel rods. Visual inspections of Assemblies 8I and 16I have not been scheduled.

A photograph of the 9I failure is shown in Figure 4. This failure consists of one major crack extending about 9 cm on each side of the peak heat flux location and several smaller cracks, which are a fraction of a cm to 6 or 7 cm long. A photograph of the 1I failed fuel rod was not obtained. Visual observations during the VBWR pool inspection indicated that the rod contained one small crack (~3 cm long) at the peak heat flux location.

Both the failures in the Type I clad have occurred in the corner rods which have a burnup about 10 percent higher than the assembly average. The failures of the Type I fuel rods are similar in appearance to those of the HPD Program that resulted from intergranular attack.[(2)]

The design characteristics and operational data of the 1I and 9I Assemblies are summarized in Table IV. Detailed examination of the failed fuel rod from the 9I Assembly is in progress. The extent of any additional examination of the failed stainless steel clad fuel rods is contingent on the results of the examination of the 9I failure. If the 9I failure is similar to those observed in the HPD Program, no additional work is considered necessary.

Type J Cladding

One Zr-4 clad fuel rod from Assembly 25J has been visually identified as a failure.

A photograph of the visually observed failure is shown in Figure 5 and the design characteristics and operational data of Assembly 25J are presented in Table IV. This failure occurred in one of the three Zr-4 clad fuel rods which were irradiated in the 25J

TABLE III

DESIGN CHARACTERISTICS AND OPERATIONAL DATA OF FAILED FUEL FOLLOWER ASSEMBLIES

	Assembly 4H	Assembly 8H	Assembly 9H
Fabrication			
Rod diameter, cm	1.07	1.07	1.07
Clad material	← Type 304 Stainless Steel →		
Clad thickness, cm	0.051	0.051	0.051
Yield strength of clad, kg/cm^2	2800	2800	2800
Type of fuel	← Sintered and ground UO_2 pellets →		
Pellet-to-clad gap, cm	← 0.0075 to 0.020 →		
Irradiation			
Average assembly burnup (fissions/cc) × 10^{-20}	2.44	2.11	2.33
Peak Assembly Heat Flux, w/cm^2	121	118	127
Hours at power of >5 MW	9946	9544	9544
Number of power cycles, 0 to >20 MW back to 0	197	196	196
Number of thermal cycles, 0 to 5 MW and back to 0	384	383	383
Failed Rod			
Rod location	← Outside, next to corner rod(1) →		
Failure location	← Near middle wire spacer →		
Type of failure	Circumferential cracks over half of circumference	Circumferential cracks with an 11-cm piece missing	Circumferential crack over half of circumference

(1) A corner rod in 4H was also failed.

TABLE IV

DESIGN CHARACTERISTICS AND OPERATIONAL DATA

FAILED TYPE I AND J BASIC ASSEMBLIES

	Assembly 1I	Assembly 9I	Assembly 25J
Fabrication			
Rod diameter, cm	1.04	1.04	1.08
Clad material	304 stainless steel	304 stainless steel	Zr-4
Clad thickness, cm	0.038	0.038	0.056
Yield strength of clad, kg/cm^2	6200	6200	3180
Type of fuel	Sintered and ground pellets	Sintered and ground pellets	Sintered and ground pellets
Pellet-clad gap, cm	0.003-0.023	0.008-0.020	0.008-0.020
Irradiation			
Average assembly burnup, (fissions/cc) $\times 10^{-20}$	1.92	2.38	1.66
Peak assembly heat flux, watts/cm^2	128	132	155
Hours at power >5 MW	7839	9390	6358
Number of power cycles, 0 to >20 MW and back to 0	152	195	94
Number of thermal cycles, 0 to 5 MW and back to 0	332	382	177
Failed Rod			
Rod location	Corner rod	Corner rod	Rod adjacent to corner rod
Failure location	Peak flux	Peak flux	53 cm above end plug.
Type of failure	Longitudinal crack about 1.9 cm long	Longitudinal crack about 17 cm long	Conical hole about 0.30 cm at outside, 0.10 cm on inside.

assembly. The failure is a conically-shaped hole about 0.3 cm in diameter at the outer clad surface and about 0.1 cm in diameter at the inner clad surface. The clad appears to be bright and shiny and there is no evidence of either a black or white oxide film on the new surface. Detailed metallography of the failure is scheduled.

Assembly 14J gave a positive sipping signal, but detailed visual examination has not yet been performed.

3. Fuel Performance Evaluation

The performance of the Type 304 stainless steel clad basic Fuel Cycle assemblies is comparable to the performance of the HPD assemblies of similar design.[2, 3, 4, 5, 6, 7] The HPD Type A, B, E, and F fuel rods, though not identical, are similar to the H and I Fuel Cycle fuel rods as shown below.[8, 9]

	HPD Rods		Fuel Cycle Rods	
	A and B	E and F	H	I
Clad Material	304 stainless steel	304 stainless steel	304 stainless steel	304 stainless steel
Yield strength of clad, kg/cm^2	2800	3200 and 6000	2900	5200
OD of clad, cm	1.078	0.915	1.078	1.041
ID of clad, cm	0.980	0.845	0.980	0.980
Clad thickness, cm	0.051	0.0355	0.051	0.038
Pellet diameter, cm	0.953	0.838	0.953	0.953
Nominal diametral gap, cm	0.013	0.013	0.013	0.013

A plot of percent of failures as a function of fuel burnup for the HPD Type E and F cold-worked stainless steel cladding is shown in Figure 6. Because of the limited number of failed HPD fuel rods clad with annealed stainless steel, a similar curve is not available. However, the limited data which are available indicate that the curve for the annealed clad is about the same as for the cold-worked clad of similar fuel rod designs.

The percent of failures as a function of burnup for the positively identified Fuel Cycle failures, 4H, 8H, 9H, 1I, and 9I corresponds very closely to that predicted by HPD failures as shown in Figure 6. (This figure has been plotted based on average exposure of each group, H or I. Alternately, it may be interpreted in terms of percentage failure in a given fuel bundle, provided only that the maximum/average exposure is comparable.) Assuming that 8I and 16I each contain a failed fuel rod is consistent with the correlation. The Fuel Cycle data indicate that there is little difference in the time to failure for the H and I Type fuel rods.

Because the HPD data correlates so well with the Fuel Cycle data, the curve shown in Figure 6 can be used to represent the performance of the H and I Type fuel rods. This curve indicates that essentially all of the fuel rods would have failed by the time the average exposure of all of the rods reached $3.17 \cdot 10^{20}$ fissions/cc (11,000 MWD/T).

C. Special Fuel Program

The Special Fuel Program includes the irradiation and examination of 12 fuel assemblies based on fuel concepts which show potential for improved fuel cycle economy through increased performance or lower fabricating costs. These assemblies will be operated at high specific power to long life to determine performance capabilities in relation to the basic fuel assemblies which represent current fuel design and fabrication processes.

The design and fabrication characteristics of the 12 Special Assemblies are listed in Table V.

The irradiation of one special assembly has been terminated previously; the current status of the remaining 11 is summarized in Table VI.

The Special Fuel Assemblies are divided into the following four groups:

1. Higher Thermal Performance

Operation of fuel at higher thermal performance improves the economics of the fuel cycle, provided that a reasonable fuel lifetime is achieved. Assembly 1L is a test of UO_2 fuel at higher temperatures while Assembly 9L provides an evaluation of thermal conductivity improvers.

2. Alternate Clad Materials

Zirconium alloys provide a low neutron capture cross section fuel clad material which has good corrosion resistance to water at temperatures normally encountered in water-cooled reactors. These alloys are susceptible to hydride embrittlement as a result of corrosion.

The austenitic stainless steels have good corrosion resistance even on the inside surface of defective fuel rods. However, the cross section of the austenitic stainless-steels is about 30 times that of Zr-2. Furthermore, the High Power Density Program and, more recently, the Fuel Cycle Program have indicated that the stainless steel clad fuel rods are susceptible to intergranular attack.

To determine whether the performance and/or fuel cycle costs using stainless steel or Zircaloy clads can be improved, the testing of fuel rods of the following concepts is in progress:

TABLE V

DESIGN AND FABRICATION CHARACTERISTICS OF SPECIAL FUEL

Element Designation	Concept	Number of Rods	Clad Material	Room Temperature Yield Strength kg/cm^2	Wall Thickness (cm)	Tube OD (cm)	UO_2 Density Percent T. D.	UO_2 Enrichment Percent	Fabrication Process	UO_2 to Cold Clad Diametral Gap (cm)
1L	Centermelt	8	Type 304 stainless steel	4360	0. 051	1. 31	94-96	3. 9 and 4. 3	S&GP	0. 010-0. 015
2L	Incoloy	8 8	Incoloy Incoloy	2810 6330	0. 051 0. 051	1. 07 1. 07	94-96 94-96	5. 46 5. 46	S&GP S&GP	0. 010-0. 015 0. 010-0. 015
3L	Incoloy	8 8	Incoloy Incoloy	3090 6330	0. 025 0. 025	1. 08 1. 08	94-96 94-96	5. 46 5. 46	SOP SOP	0. 00 0. 00
4L BMI	Isostatic pressed	3	Type 304 stainless steel	Ann.	0. 043	1. 02	96	5. 58	IS	0
4L UNC	Low temperature sintered pellets	3	Type 304 stainless steel	5690	0. 038	1. 02	95-96	5. 0	LTSP	0. 008-0. 020
4L	Centermelt calibration	1	Type 304 stainless steel	2810	0. 165	3. 49	94-97	3. 9	S&GP	0. 025
5L	Coextruded UO_2 and stainless steel clad	12	Type 304 stainless steel	Ann.	0. 038	1. 02	97-99	5. 5	Ex F&C	0
6L	Zr-4	16	Zr-4	4430	0. 069	1. 44	94-97	3. 9	S&GP	0. 015
7L	Stainless steel lined Zr-2	12	Stainless steel lined Zr-2	4220	0. 058	1. 07	94-97	4. 58	S&GP	0. 010-0. 015
8L	0. 013 cm stainless steel clad pellets	8 4	Type 304 stainless steel Type 304 stainless steel	6120 2950	0. 013 0. 013	0. 965 0. 965	94-97 94-97	4. 58 5. 0	SOP	0
9L	Thermal conductivity improver	8	Type 304 stainless steel	6190	0. 051	1. 31	89-95	5. 46, 6. 5 and 8. 0	S&GP	0. 005-0. 010
10L	0. 013 cm stainless steel clad powder	8 8	Type 304 stainless steel Type 304 stainless steel	2950 6330	0. 013 0. 013	0. 965 0. 965	83-85 83-85	6. 0 6. 0	VCP VCP	0 0
11L	Extruded UO_2	16	Type 304 stainless steel	5830	0. 056	1. 37	97-99	5. 5	UO_2 Exn	0. 010-0. 020
12L	Burnable poison	16	Type 304 stainless steel	2810 6330	0. 028 0. 028	1. 23	85 and 93-95	5. 5 and 6. 6	S&GP and VCP	0 and 0. 008-0. 010

(1) S&GP = Sintered and ground pellets
SOP = Swaged over pellets
IS = Hot gas isostatic pressed fuel and clad
LTSP = Low temperature sintered pellets
Ex F&C = Extruded fuel and clad
VCP = Vibratory compacted powder
UO_2 Exn = UO_2 extrusions

TABLE VI

SUMMARY OF OPERATIONAL DATA OF SPECIAL FUEL ASSEMBLIES

Element Designation	Peak Surface Heat Flux Watts/cm^2	Peak Surface Heat Flux Btu/hr ft^2 × 10^{-3}	Peak Fuel Center Temperature °C	Burnup Fissions/cc × 10^{-20}	Burnup MWD/T	Hours at >5 MW	Power Cycles 0 to 20 MW Back to 0	Thermal Cycles 0 to 5 MW Back to 0	Comments
1L	151	480	2650	1.87	6487	6867	123	211	
2L	105	335	--	0.24	833	835	5	5	
3L	135	430	1760	0.39	1353	2027	21	27	
4L BMI	118	375	1649	0.09	316	439	11	18	Failed
4L UNC	105	334	--	0.80	2847	3151	36	42	
4L CC	168	533	2760	0.04	147	439	11	18	Work completed
5L	140	446	1782	2.11	7327	8044	157	250	Weak sipping signal
6L	128	407	2538	0.89	3091	4805	84	94	Cracked end plug weld
7L	147	467	2343	1.94	6751	6834	117	171	
8L	154	488	2093	1.38	4795	6076	98	158	Failures at 0.76 and 1.38 × 10^{-20} fissions/cc
9L	125	396	Unknown	0.93	3216	3170	61	62	Weak sipping signal
10L	110	350	1482	1.03	3591	3933	60	64	Collapsed at plenum; weak sipping signal
11L	125	398	2150	0.70	2428	3151	36	42	
12L	132	418	1870	0.86	2972	3933	61	62	

a. Provide protection to the inside surface of Zr-2 tubing - Assembly 7L.

b. Improve the hydride resistance of zirconium alloys - Assembly 6L.

c. Reduce the thickness of the stainless steel clad to a thin shell - Assemblies 8L and 10L.

d. Improve the resistance of the stainless steels to intergranular attack - Assemblies 2L and 3L.

3. Reduced Fabrication Cost Concepts

Irradiation of assemblies containing fuel rods made by new fabrication processes, which offer potential increases in UO_2 density or cost reductions in the manufacture of UO_2 fuel elements, will provide engineering proof tests of the feasibility of these new methods. The testing of fuel rods fabricated by the following methods is in progress:

a. Low temperature sintered pellets - Assembly 5L.

b. Co-extruded UO_2 and stainless steel clad - Assembly 5L.

c. UO_2 extrusions - Assembly 11L.

4. Extended Life Concepts

The loss of reactivity as the result of fuel burnup may limit the life of the fuel. Initial reactivity for burnup is limited by the capacity of the control system to make the cold, clean core subcritical. The reactivity change associated with the fuel burnup can be reduced by burnable poisons. Assembly 12L is designed to evaluate boron as a burnable poison by: 1.) alloying boron with the stainless steel cladding, and 2.) mixing a boron compound with the UO_2.

The irradiation of the self supporting Incoloy clad Assembly, 2L, began with VBWR Run 164, and it continues to operate satisfactorily.

The in-core sampler during VBWR Run 165 and sipping following Run 165 indicated that Assemblies 6L and 8L may contain defective fuel rods. All other special assemblies continued to operate satisfactorily.

Visual examination of the Zr-4 clad Assembly 6L, in the VBWR pool revealed that corner Rod C-4 contained a circumferential crack in the weld at the bottom end plug. A photograph of this crack is shown in Figure 7, and the design characteristics and operational data of the assembly are presented in Table VII. The white corrosion product on the fuel rod as shown in Figure 7 is believed to be hydrated alumina adhering to the surface rather than zirconium oxide. The hydrated alumina is a corrosion product from the VBWR pool hardware.

TABLE VII

DESIGN CHARACTERISTICS AND OPERATIONAL DATA OF FAILED FUEL RODS FROM THE SPECIAL ASSEMBLIES

	Assembly 6L	Assembly 8L Cold-Worked	Assembly 8L Annealed
Fabrication			
Rod diameter, cm	1.44	0.965	0.965
Clad material	Zr-4	304 stainless steel	304 stainless steel
Clad thickness, cm	0.069	0.013	0.013
Type of fuel[1]	S&GP	SOP	SOP
Pellet to clad gap, cm	0.0075 to 0.020	0.000	0.000
Irradiation			
Average assembly burnup (fissions/cc) $\times 10^{-20}$	0.89	1.38	0.64
Peak assembly heat flux, watts/cm^2	128	154	108
Hours at power of >5 MW	4805	6076	2574
Number of thermal cycles, 0 to 5 MW and back to 0	94	158	30
Number of power cycles, 0 to >20 MW and back to 0	84	98	25
Failed rod			
Rod location	Corner	Unknown	Unknown
Failure location	End Plug Weld	Unknown	Unknown
Type of failure	Circumferential crack extending about 1/3 of circumference	Unknown	Unknown

[1] S&GP = Sintered and ground pellets
SOP = Swaged over sintered and ground pellets

Some difficulties were encountered in the welding of the lower end plugs during the fabrication of the fuel rods. Detailed metallographic examination of the welds from a rejected fuel rod did not reveal any defect which might cause the type of cracking observed in Rod C-4. A few voids in the weld zone were observed, but these voids were very small and none of them penetrated the complete weld zone. Additional information which may reveal the cause of cracking will be obtained by detailed destructive examination of the failed fuel rod at RML.

Examination of the 0.013-cm wall stainless steel clad swaged over pellet assembly (Assembly 8L) in the VBWR pool revealed that the five fuel rods clad with annealed stainless steel had wrinkled as shown in Figure 8. The wrinkles were not limited to the peak heat flux region, but generally ran the entire length of the fuel rods. It was impossible to locate any holes or cracks in the clad during the pool examinations. Detailed visual and metallographic examination which is scheduled for early 1964 should determine whether there are any cracks in the wrinkles. The design characteristics and operational data of the 8L Assembly and these fuel rods are presented in Table VII. The five fuel rods clad with fully annealed stainless steel replaced the fuel rods clad with cold-worked stainless steel which were removed in August, 1962.

The 0.013-cm wall stainless steel clad powder fuel assembly (Assembly 10L), was visually examined at an exposure of about 0.7×10^{20} fissions/cc. The examination revealed the following:

1. The clad has been pinched and wrinkled by the external operating pressure in the area just below the plenum support tube. A typical example of this wrinkling and pinching is shown in Figure 9. The wrinkling was observed in varying degrees on eight of the 16 fuel rods. The cause of the clad deformation is suspected to be a reduction in powder density in this region and consequently loss of adequate clad support.

2. One corner rod had a series of scratches near the peak heat flux zone which appeared to be between 0.002 and 0.005 cm deep.

Because there were no indications of failure, either by visual examination or by sipping techniques, the assembly was returned to the VBWR for Run 166.

Following the final VBWR run (Run 166), weak activity release signals were obtained from sipping tests on Assemblies 5L, 9L, and 10L.

During this quarter, GEAP-4408, "A Uranium Dioxide Fuel Rod Center Melting Test in the Vallecitos Boiling Water Reactor," by H. E. Williamson and J. P. Hoffmann, November, 1963, was issued. The summary of the report is as follows:

As part of the AEC Fuel Cycle Program, tests are being conducted to evaluate the significance of current fuel design limitations that do not permit the maximum fuel temperature to exceed the melting point of UO_2. The reliability of prediction of the fuel rod operating conditions that will cause melting of the UO_2 was evaluated by means of a calibration test conducted in the VBWR.

The calibration test rod characteristics are summarized below.

CALIBRATION ROD DESIGN

UO_2 Pellet Diameter	3.145 ±0.008 cm
Pellet-to-Clad Diametral Gap	0.01 - 0.025 cm
Clad Material	304 stainless steel, 1/4 hard
Clad Outside Diameter	3.5 cm
Clad Thickness	0.165 cm
Active Fuel Length	89 cm
Fuel Enrichment	3.9 percent U-235
Pellet Density	96-98 percent of theoretical

Irradiation of the calibration rod was begun on December 21, 1961, in a core position which resulted in a peak surface heat flux of 73.5 watts/cm^2. [The VBWR-AEC operating license requires that new fuel assemblies be operated below 79 watts/cm^2 (250,000 Btu/hr-ft^2) and inspected prior to operation at design power.]

The calibration rod was then moved to a core position where a heat flux up to the burnout safety margin limit, 173 watts/cm^2 (548,000 Btu/hr-ft^2), could be achieved. Immediately after reactor startup, the calibration rod was taken to a heat flux of 143 watts/cm^2; this heat flux was maintained for 6 days. During this run, the reactor power was increased 10 to 20 percent for three separate subruns, to attain the desired center-melting; the subruns are summarized in the following table. The reactor was shut down immediately following the last subrun. (A histogram of the test fuel rod operation is shown in Figure 1 of GEAP-4408.)

CALIBRATION ROD OPERATION

RUN 138

Run	Date	Time (Hours)	Rod Peak Heat Flux (watts/cm^2)
A	1/7/62	2	155
B	1/10/62	4.28	155.5
	1/11/62	0.87	155.5
		0.5	161
		2.1	169
C	1/12/62	2	155

Following this irradiation, the fuel rod was transferred to the RML for detailed examination which consisted of the following:

1. Gamma-scanning the rod.
2. Checking the cladding OD dimensions.
3. Measuring the cladding thickness.
4. Sectioning the rod.
5. Performing visual examination of the cut sections to determine the extent of grain growth and void formation.
6. Performing a burnup analysis.
7. Performing metallographic examination of the fuel and clad.
8. Performing autoradiography on the metallographic specimens.

(The appearance of the calibration rod sections is shown in Figures 1 and 15 of GEAP-4408.) Observations indicate that centermelting of the UO_2 has occurred. At the highest neutron flux location, which is 25 to 30 cm from the bottom, the uranium dioxide is solid except for cracks and a small void probably formed by contraction from freezing. The central void increases in diameter about 46 cm from the bottom of the fuel, and extends for approximately 34 cm to within about 8 cm from the top of the fuel column. The maximum diameter of the void is approximately 1.5 cm. The uranium dioxide must have melted and flowed from the upper part of the rod to the lower part.

The gamma scan usually provides a map of operating power distribution, but in this test the gamma activity distribution was apparently affected by the redistribution of the uranium dioxide. Consequently, the power distribution along the length of the rod was estimated from power distributions obtained from previous experiments in the VBWR.

Considerable plastic deformation of the cladding tube, as a result of operation, was evidenced by a reduction of approximately 0.75 mm in the outside diameter of the tube. High residual stresses in the clad were indicated by expansion ("belling") of the tube as the sections were cut. Localized thinning of the clad in the order of 0.25 to 0.38 mm was noted from detailed examination of three sections. Precise post-irradiation measurements of rod length were not obtained, but length changes consistent with the above cladding changes were not apparent. At the peak power location the thermal expansion of the pellets created a calculated clad diametral strain of 2.6 percent. This strain corresponds to a stress level of approximately 1.97×10^3 kg/cm^2 (28,000 psi).

Conclusions

1. The central portion of the 3.15-cm-diameter uranium dioxide fuel column melted. It appears that the UO_2 was molten out to a radius of 1.22 cm in the peak power region. The maximum extent of melting probably occurred during the peak power run when the $\int_{T_o}^{T_c} kdT$ in this region of the rod reached 171 watts cm.

   The estimated radius of melting from metallographic examination indicates the $\int_{T_o}^{T_m} kdT$ for sintered UO_2 is 59 watts cm. This supports a calculated estimate for sintered UO_2 thermal conductivity published by D. R. deHalas and G. R. Horn.[10] The results of the previous calibration run[11] and subsequent experimental data by Lyons[12] are also consistent with this value. This conclusion is contingent on the interpretation of the post-irradiation crystal structure of the UO_2. Insufficient data are available on the mechanisms by which various UO_2 crystal structures are formed to permit a positive identification of the extent of melting and correlation with time of operation. No conclusion can be drawn as to whether the thermal conductivity of the UO_2 changed with operation.

2. Although extensive UO_2 melting occurred, there was no indication of fuel rod clad failure.

3. Axial heat transfer by convection in the molten UO_2 was significant.

D. Stability

This task provides for the development of a mathematical stability model to predict the dynamic performance of boiling water reactors, and for stability tests in the VBWR and experiments in a stability loop to provide an experimental basis for the model. The work on this task was terminated in May, 1963, except for completion of terminal reports.

The major report on the stability work has been completed, thus concluding this task:

GEAP-3971, "VBWR Stability Test Report," by Members of Engineering Development, June,1963, (released January 1964).

GEAP-3971 is a summary of preliminary work on an extensive series of power stability tests which were conducted in the VBWR during November and December, 1961. Tests were conducted with both natural and forced circulation coolant flow over a wide range of flows and powers. The tests were planned as a result of the need for establishing a basis for predicting the transient responses and stability of power producing BWR's. Such a study for these reactors requires theoretical and experimental identification of the events leading to instability and to determine methods of obtaining non-noisy steady-state operation of BWR's.

The economic incentive for such an investigation has been a strong one since improved economics is indicated to come from increased power output, shorter piping loops, and lower flow rates. The general effect of these design changes is to decrease the margins of safety for stability. The definition of such margins is very poorly known since defined limits for safe operation are not accurately known.

The stability task of the Fuel Cycle Stability Program has addressed itself to initial work in this task. A theoretical study to describe the stability responses of the VBWR was carried out for these tests and the experimental results compared with this theory. The experiments were obtained in a well-instrumented reactor facility and provide a basis for a more generally useful and improved analytical model.

The VBWR reactor was instrumented, in addition to regular process instruments, to include five* assemblies with the provision for measuring inlet flow rate, neutron flux at three axial core locations, pressure drop, and temperature. Test data was recorded on oscillograph recorders and magnetic tape.

The VBWR was designed specifically for this type of experiment. A wide range of operating conditions is permitted with the same core. Tests were conducted as follows:

Forced Circulation		
Power	MWt	1, 15, 20, 26
Flow	gpm	2600 to 20,000
Pump Head	ft	0 to 290
Core Bypass Leakage % of Core Flow		0 to 400
Natural Circulation		
Power	MWt	9 to 20

Theoretical analyses of the dynamic responses were used to guide the experimental parametric study. Analysis was conducted by average parameter control system analysis techniques, and solutions were obtained on an analog computer. The system representation includes reactor kinetics, fuel thermal responses, thermal-hydraulic responses, and void reactivity response. Thermal-hydraulic response analysis, which is unique to this investigation, consists of solutions of the equation of motion, continuity, energy, and fluid transport time. These equations are evaluated representing the reactor as a single (point) node.

*Two belonged to the Consumers High Power Density Research and Development Program.

ANALYTICAL MODEL OF VBWR RESPONSES

The logic block diagram for system analysis of VBWR responses is shown below. The analytical model is described in detail in references (13), (14), (15), and (16).

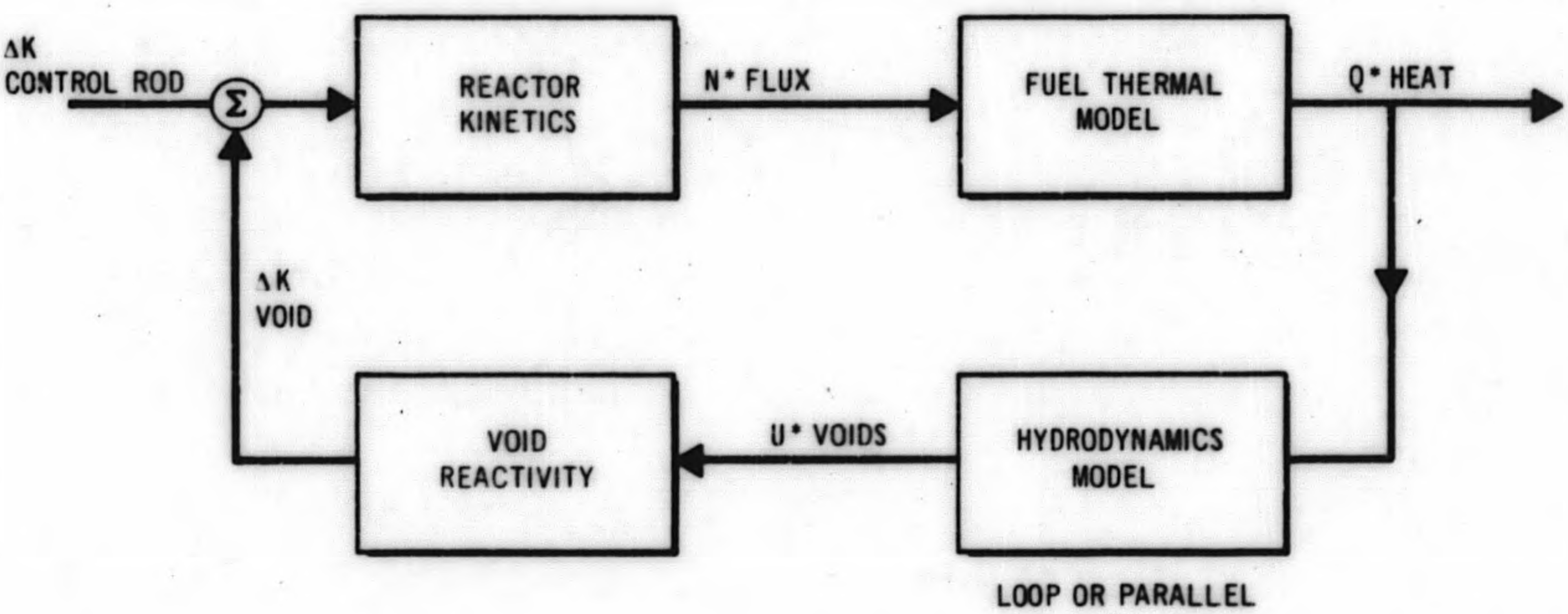

The averaged parameter solutions for neutron kinetics are obtained from a nonlinear representation of the conventional six delay group thermal fission model. The equation representing this simulation is:

$$\frac{N^*}{\Delta K} = \frac{1}{s\left[\tau_o + \sum_{i=1}^{6} \frac{\beta_i/\beta}{(s + 1/\tau_i)}\right]}$$

where N^* is the nomalized flux response
ΔK is the reactivity
s is the complex frequency
τ_o - the quantity l^*/β^*
l - neutron lifetime - sec
β_i - delayed neutron group fraction
τ_i - decay constant

The fuel thermal model simulation was a linear transformation of the thermal diffusion equation which related heat imported to the fluid at the surface of the fuel element Q^* (in normalized values) to neutron density (N^*). This relationship is based upon a transient analysis of the temperature and heat transfer characteristics of a cylindrical rod with internal heat generation [reference (17)]. The form of this transient expression is a four-node series approximation of varying heat flux path length to clad surface.

$$\frac{Q^*}{N^*} = \frac{0.826}{1 + 6.38(s)} + \frac{0.104}{1 + 1.16(s)} + \frac{0.038}{1 + 0.296(s)} + 0.032$$

The hydrodynamics model is derived from the solution of the equation of motion, energy, continuity, and a boundary condition upon two-phase flow. The force balance for the water pressure gradient is:

$$(1 - u)\frac{\delta P}{\delta x} + \frac{\delta}{\delta x}(1 - u)\rho_w W^2 + \frac{\delta}{\delta t}(1 - u)\rho_w W + \Gamma_w - \Gamma_{ws} + (1 - u)\rho_w g = 0$$

For the steam force balance:

$$u\frac{\delta P}{\delta x} + \frac{\delta}{\delta x} u\rho_s s^2 + \frac{\delta}{\delta t} u\rho_s S_s + \Gamma_s + \Gamma_{ws} + u\rho_s g = 0$$

For conservation of mass:

$$\frac{\delta}{\delta x}(1 - u)\rho_w W + \frac{\delta}{\delta t}(1 - u)\rho_w + \frac{\delta}{\delta x} u\rho_s S + \frac{\delta}{\delta t} u\rho_s = 0$$

The conservation of energy is expressed as:

$$\frac{\delta}{\delta x}(1 - u)\rho_w W h_w + \frac{\delta}{\delta t}(1 - u)\rho_w h_w + \frac{\delta}{\delta x} u\rho_s h_s + \frac{\delta}{\delta t} u\rho_s h_s = g(x, t)$$

These equations are applied assuming:

1. Steam and water are in saturated equilibrium.
2. Flow process is adiabatic.
3. Transverse gradient is negligible with respect to axial pressure gradient.
4. Shear stress between phases and between each phase and the wall are analytic functions of the phase velocities, the phase volume fractions, and flow rate ratios.
5. The flow system pressure drop is small enough compared to the absolute pressure that saturation enthalpies and densities are constant.
6. Fluid mechanical energy is small compared to the thermal energy.

These equations are integrated along the length of the channel, and with the addition of two equations which define boundary conditions the equations, without second order effects, become:

Momentum steam and water:

$$\frac{1}{\rho_w}\left(\frac{\Delta P}{\Delta x}\right) + \left[\frac{1 - R}{2L}(w^2 - v^2)\right] + (1 - R)\frac{dW}{dt} + (1 - R)g + \frac{G_w W^2}{2} = 0$$

Momentum Steam: $$\frac{1}{\rho_w}\frac{\Delta P}{\Delta x} + G_{ws}\left(\frac{1-R}{2}\right)[s-w]^2 = 0$$

External Loop: $$\frac{1}{\rho_w}\left(\frac{\Delta P}{\Delta x}\right) + g - \frac{K}{L}\frac{v^2}{2} - \frac{L_D}{L}\frac{dv}{dt} = 0$$

Energy and Continuity:
(Volume)
$$\left(1 - u(o,t)\right) W(o,t) + u(o,t)\, S(o,t) = \gamma\,(\beta-1) + v(1+\alpha-\alpha\beta)$$

Energy and Continuity.
(water flow boundary condition)
$$\left(1 - u(o,t)\right) W(o,t) = v(1+\alpha) - \gamma$$

$$R = \frac{1}{L}\int_0^L u\,dx \sim \frac{1}{L}\int_{t-\frac{L}{w}}^{t} u\,W\,dt$$

The above equations are normalized, linearized, frequency transformed, and solved. Hydrodynamics equations were solved by use of a digital code and expressed as analog inputs to a system analog representation as in Figure 10.

The void reactivity model used was a linear relationship which describes the excess reactivity due to steam volume changes within the core (ΔK void) that are caused by reactor heat. This is a transport relation which averages the core steam volume in time and assigns a void worth of reactivity to that average. The void reactivity gains were determined from reactivity calculations of the core employed for the tests.

$$\frac{\Delta K \text{ void}}{u^*} = \frac{\text{Void Worth}}{1 + \frac{\tau_c (s)}{2} + \frac{\tau_{(c)}^{\,2} (s)^2}{12}}$$

Here the numerical value of τ_c must be determined for each operating condition of the reactor because it, like the hydrodynamic model, is a linear approximation of a nonlinear relationship.

RESULTS

The extensive testing performed in the VBWR has only been examined in detail for five runs which represent the best parametric comparison of theory and experiment that could be obtained from the data. The data has been analyzed with bandpass filter equipment which represented the best analysis method available at the beginning of the program. Subsequent investigations have shown that the quality of results produced could be improved by more sophisticated methods: for example, digital codes and Fourier spectral analyzers.

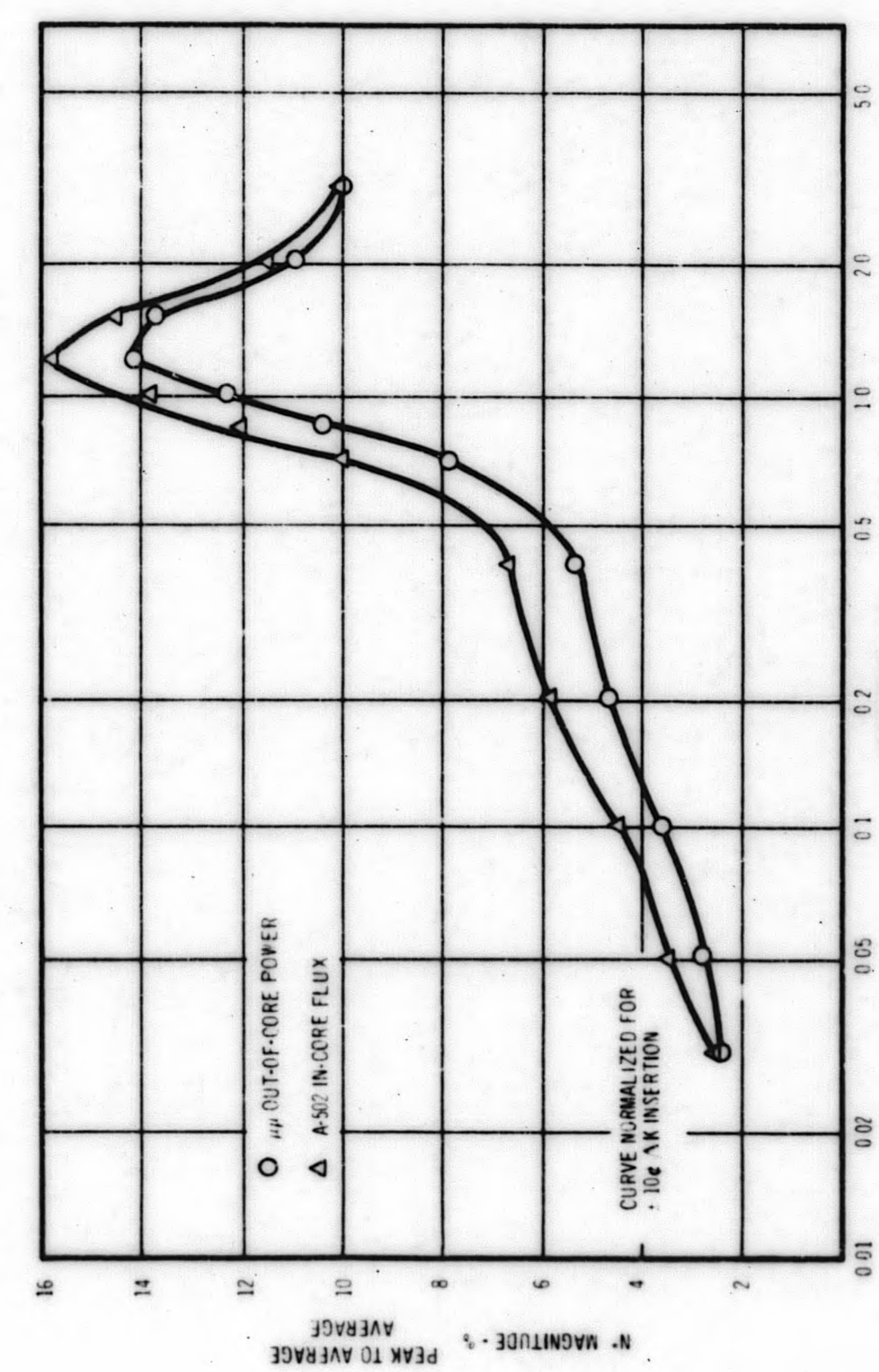

Figure 10a. Normalized Rod Oscillator Response Curve for the Speed Controlled 4,000 gpm Test Series (15-19) 15 MWt

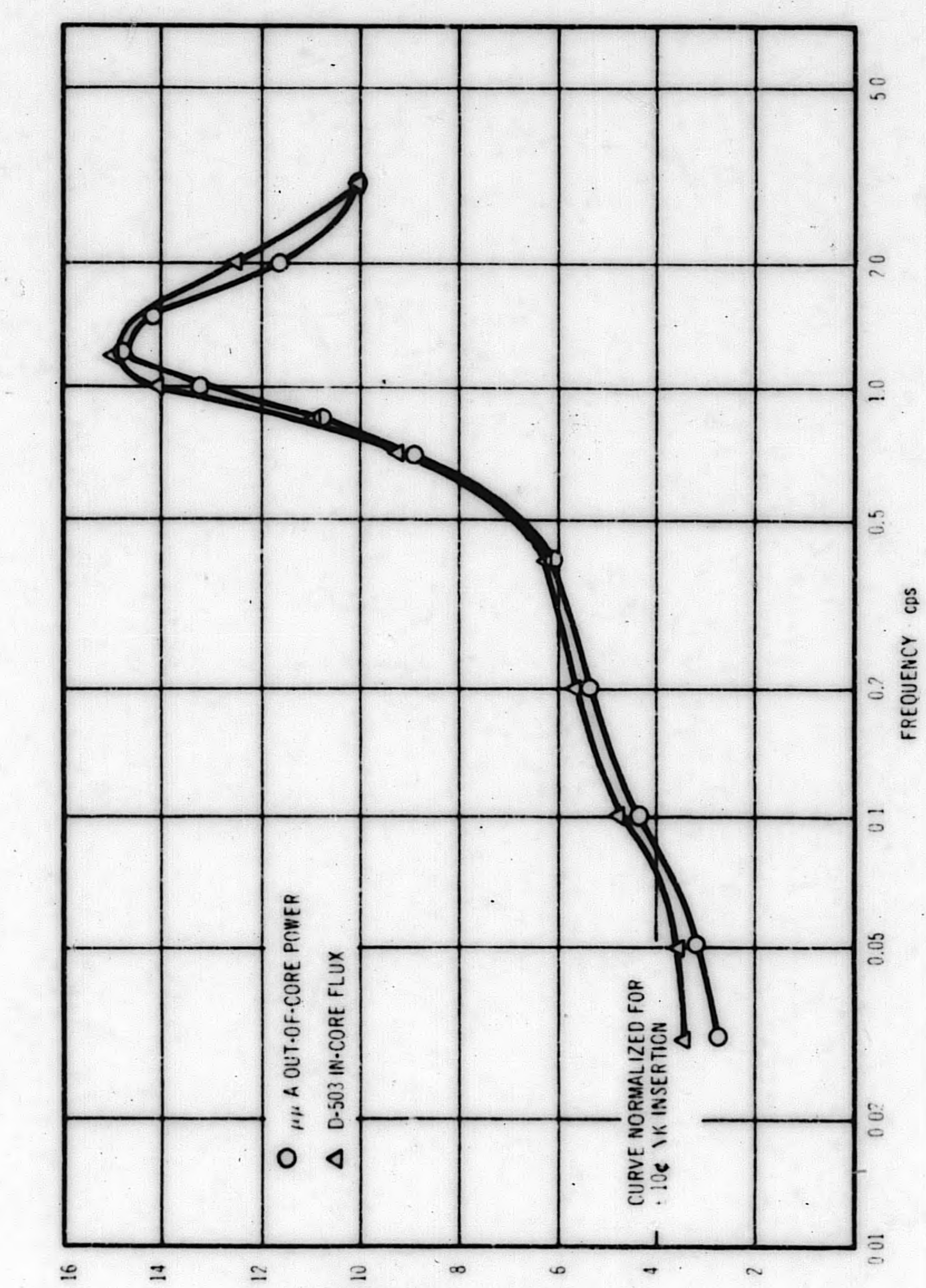

Figure 10b. Normalized Rod Oscillator Response Curve for Valve-Controlled Forced Circulation 4,000 gpm Test Series (15-9) 15 MWt

Prior to the testing, an extensive pre-test analysis of the reactor responses was conducted. These pre-test analyses were used to guide in establishing the test conditions and have served as a basis for comparison of the test data. Improved methods, both of data analysis and system analysis, are recommended to obtain maximum b nefit from the tests.

1. Rod Oscillator Tests

Rod oscillator tests were concluded to be the well-founded source of quantitative information from the VBWR tests. The pre-test analysis was conducted for two modes of thermal hydraulic oscillation: the oscillation of the entire loop, which will be designated as loop analysis; and the oscillation of thermal-hydraulically uncoupled parallel channels, or parallel channel analysis. Provision was made in the hydrodynamic response code to accomplish these two solutions.

The shapes of the power transfer functions as measured by the in-core ion chambers and the vessel external micromicroammeter flux monitor are essentially identical for a given test condition. The micromicroammeters were employed for the power response results discussed below unless otherwise designated.

a. Power Responses with Well-Damped Loop Hydrodynamics

Two reactor conditions were examined with well-damped forced circulation hydraulics, as shown below:

Power	Run No.	Flow	Comment
15 MWt	15-1	20,000 gpm	Maximum Forced Circulation
15 MWt	15-9	4,000 gpm	High Head, Valve Controlled Flow
15 MWt	15-19	4,000 gpm	Low Head, Speed Controlled Flow

The two 4000 gpm runs produced almost identical transfer functions. This indicates that the system is well-damped even in the most frictionless conditions that can be operationally produced with the forced circulation loop.

The experimental power transfer functions for the 4000 gpm case were compared with loop analysis results. Analysis and test results show comparable transfer function curves at this flow, and indicate that the system responses are loop hydrodynamic responses for the low flow, closed circuit, forced circulation mode of operation. Increasing the flow rate from 4000 gpm to 20,000 gpm, it was observed that the resonant frequency of the power transfer function increases with increasing flow. The flow dependence is, however, shown not to be large. The flow dependence predicted by pre-test analysis showed much larger changes in frequency. A much refined evaluation of the differences between theory and experiment must be obtained to evaluate the real descrepancies of theory and experiment. These differences are felt to be real and are thought to be accounted for by definite aspects of the theory.

The evaluation of the average channel responses, improvement of the void coefficient of reactivity determination, and the inclusion of a multi-node thermal-hydraulics representation in the analysis model are the primary factors which are believed to be an influence in aligning theory and experiment. The theory employed in the pre-test analysis does not provide a satisfying representation of the average channel, or average parameter to be employed in the analysis. An uncertainty remains as to the weighting of the different channels, and channel locations, upon the measured power responses.

When power transfer functions for low flow rate, closed circuit, forced circulation runs, and the corresponding high flow runs are compared (Figures 10, 11, and 12), it is found that the low flow runs show resonance peaks which have large amplitudes compared to the high flow runs. This difference has been attributed to the difference in the void coefficient $\left(\frac{\Delta K}{\beta} / \frac{\Delta R_g}{R_g}\right)$ at the two steam void levels resulting. The void coefficient of reactivity, it is concluded, is a major contribution to the stability and transient response characteristics.

No resonant hydraulics were observed in any of the closed flow circuit, forced circulation rod oscillator tests when employing the bandpass filter network. Subsequent analysis not reported in GEAP-3971 shows some effect of hydraulic resonance. The method of analysis in this second data analysis is the Boonshaft-Fuchs Fourier Spectrum Analyzer. The fluid dynamics for this mode of operation was concluded to be stable and damped for all cases investigated.

The amplitude of recorded flow noise, compared to the amplitude of oscillation of flux during the rod oscillator runs, was always small. The ratio of the variations of flow to the variation of flux varied from 10 percent of flux noise during the low flow runs to 25 percent at the 20,000 gpm test point. This points up the lack of response of the flow to rod oscillation.

The stability gain margin, the constant by which the experimental gain at 180° phase lag must be multiplied to equal one (condition for instability), is shown to decrease with increasing core voids. Therefore, the stability of the VBWR system is seen to decrease with increasing voids. This is in accordance with the trend of the pre-test analysis.

The total power reactivity feedback gain and the void coefficient of reactivity both increase with increasing core voids. This is also in accordance with the trend of the theory.

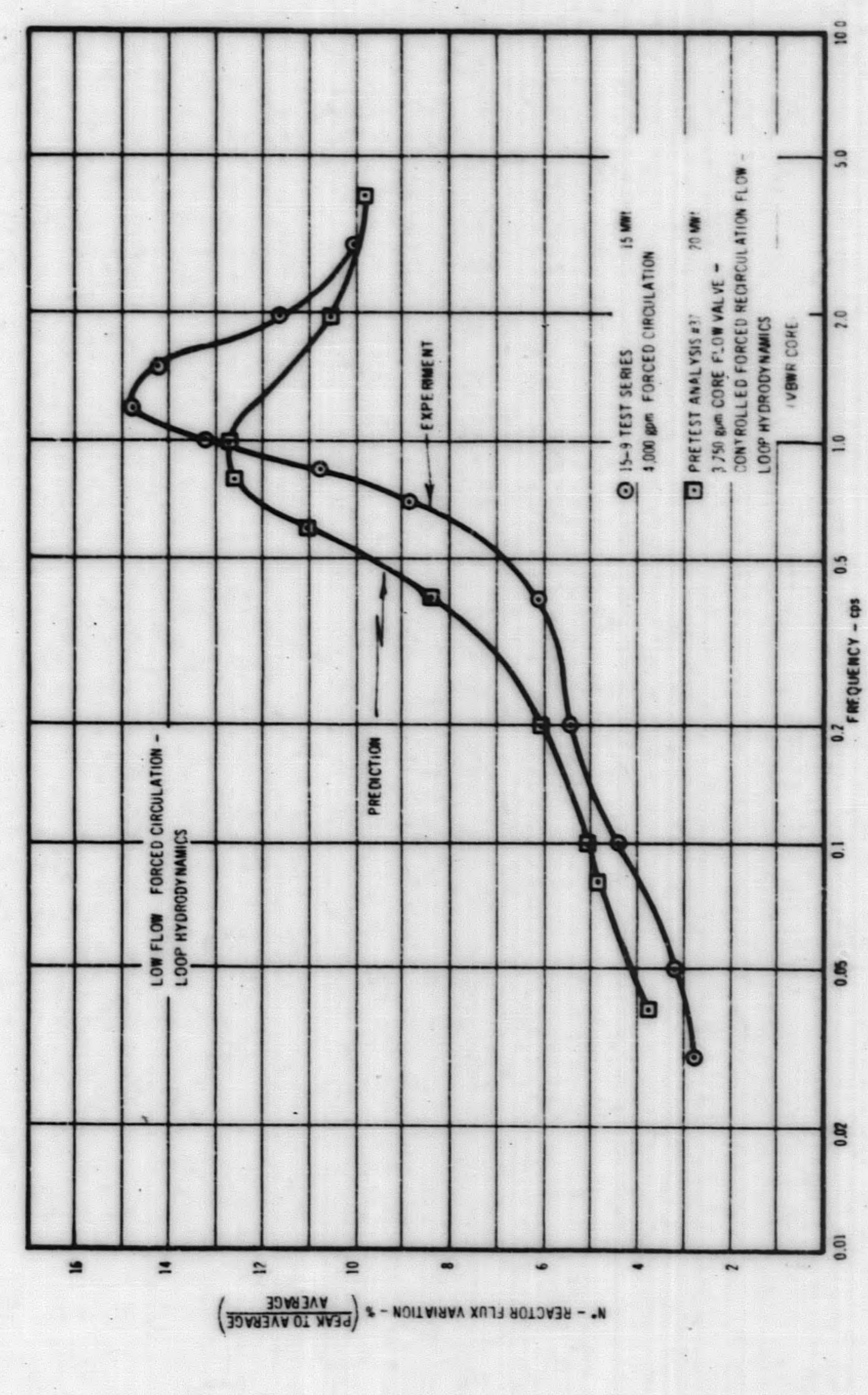

Figure 11. Reactor Power Transfer Function Comparison of Prediction with Experiment

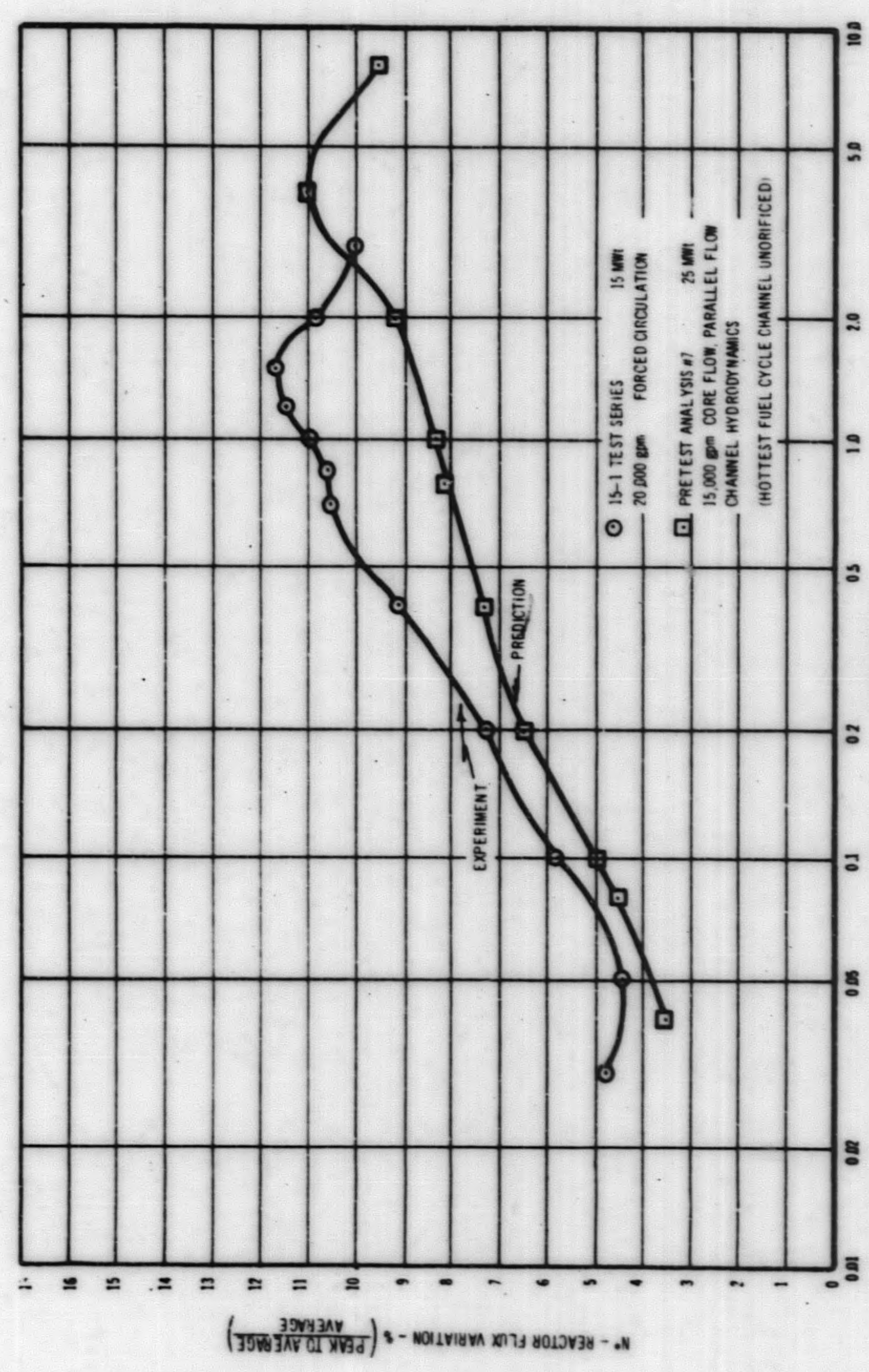

Figure 12. Reactor Power Transfer Function Comparison of Prediction with Experiment High Flow - Forced Circulation

b. Power and Flow Responses with Under-Damped Hydraulics Natural Circulation and Forced Circulation Bypass Flow

Two reactor conditions were examined under these conditions:

(1) Natural circulation within the reactor vessel at 15 MWt (Run 15-18) (Figure 13).

(2) Forced circulation at 4,000 gpm and 15 MWt with the baffle doors open (Run 15-17) (Figure 14).

The natural circulation test (15-18) and the forced circulation with baffle doors open test (15-16) have power transfer functions of similar shape. It is reasoned that the baffle door passage is large enough that bypass flows, either positive or negative, do not appreciably alter the effective single-phase gravity driving head which exists across the core in natural circulation.

Resonant hydraulics at 0.4 - 0.5 cps were exhibited within the reactor core for both the natural circulation test and the forced circulation test with baffles open. The flow resonance was demonstrated in two ways. First, by observation of the unorificed instrumented assemblies' turbine flowmeter; and second, by the existence of a characteristic dip in the power transfer function. This dip is not seen in the closed loop, forced circulation tests when analyzed by the bandpass filter or by the pre-test analysis for the loop-type mode of oscillation. It is shown, however, by the parallel channel analysis of the core channels. It is concluded that these two tests are examples of a reactor core with uncoupled parallel flow channels and strong nuclear coupling.

The effect of inlet orificing on fuel elements is to damp flow oscillations or response. This was observed from a comparison of the flow response of the unorificed and orificed assemblies during the natural circulation rod oscillator test.

2. Transient Tests

Although the transient test techniques, in theory, should provide the same information that the rod oscillation tests provide, in the practical case this is not true. Transient tests of the VBWR are considered to provide no essential information which is of value in quantitative determination of the power stability and transient responses of the VBWR. There are several reasons for this. The most basic one is due to the fact that one cannot practically retrieve much information from the response of a few seconds duration without introducing errors in data analysis and the mathematical description of events. More practically, two important limitations appeared from the fact that test conditions

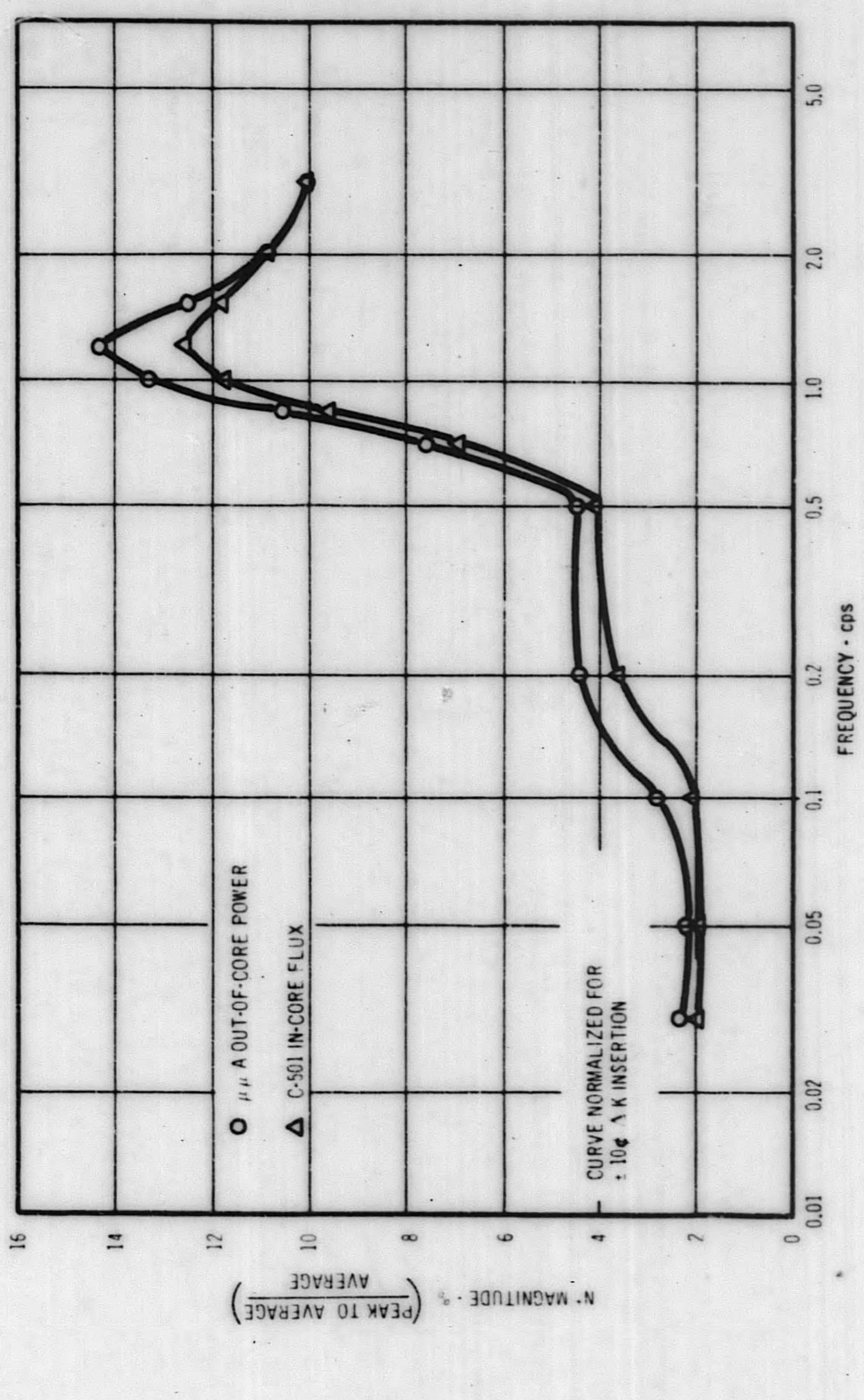

Figure 13. Normalized Rod Oscillator Response Curve For Natural Circulation Test Series (15-18) 15 MWt

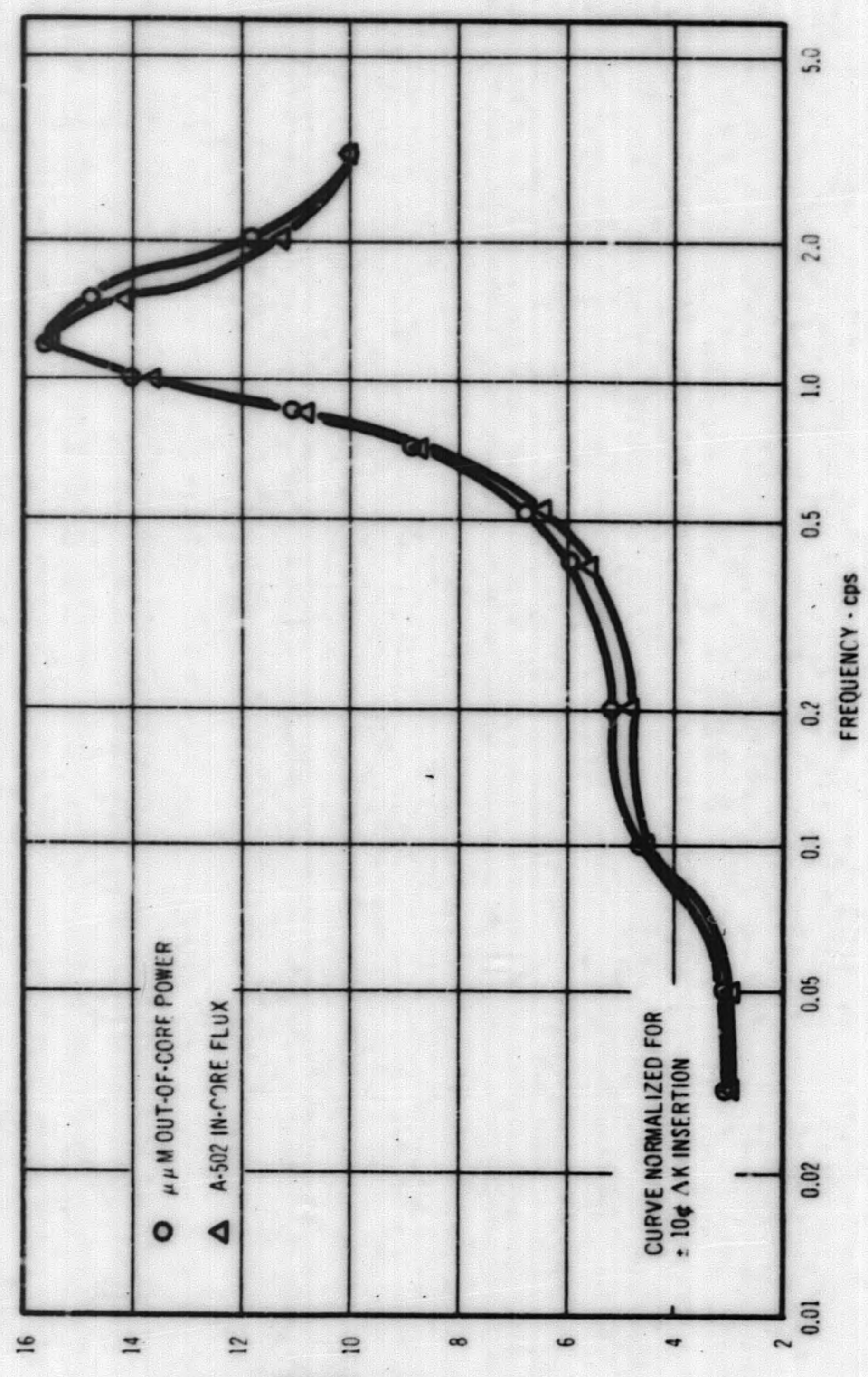

Figure 14. Normalized Rod Oscillator Response Curve for Forced Circulation Baffle Doors Open Test Series (15-16) 15 MWt

that demonstrated satisfactory stability and transient response characteristics emphatically could not be obtained, and that noise components served to obscure the results.

3. Steady-State Tests

a. It was observed that during steady-state operation, the amplitude of flux noise was affected relatively little by power level changes, but affected more by flow changes. Increasing the flow rate increased the amplitude of flow noise. This observation is of considerable importance in that it points out that the largest amplitude noise occurs at the point adjudged to be most stable. Rod oscillation tests and theory both show that at low flows the reactor is nearer a point of instability than at the higher flow point. The amplitude of flow noise for forced circulation tests in the VBWR, therefore, shows an erroneous indication of stability. On this basis, the operational amplitude of oscillations is questionable as a source of stability information.

b. The peak frequencies obtained from the output of the bandpass filter for flow and power do not show the same parametric change demonstrated by theory. Additionally, the responses are not well-defined functions of frequency. The frequency responses shown indicate that as the flow increases the peak frequency change of test observation is substantially less than expected from theory. Work subsequent to the Fuel Cycle Stability Program shows considerable inaccuracy in the bandpass for noise analysis, particularly at low frequencies.

c. Steady-state flux oscillations at frequencies of 1 cps and below were in-phase over the core. Oscillations at 2 cps and above did not show a relationship between different core locations.

d. No interrelationships can be seen in the fluxes and flows. This observation may be because of the spatial averaging of fluxes, or because of a combination of both spatial averaging of fluxes and the random responses of channels.

e. It was previously mentioned that flow oscillations in response to control rod oscillation were obtained near the resonant frequency of the system during natural circulation operation. At all other frequencies, the flow noise was far greater than the flow response to power. The flow response to power, even at the resonant frequency, was not to increase the amplitude of flow noise by adding a sympathetic flow component to power, but, rather, to cause the existing flow noise to become "ordered" with power variations; i. e., the amplitude of the flow noise at this frequency was essentially the same during the rod oscillations as it was just under the influence of steady-state noise. The foregoing observation led to the following important conclusion:

If the relatively large scale power disturbance induced by rod oscillation just barely caused a noticeable ordering of the flow noise, then the equivalent noise distrubances must be at least as large as, if not larger than, those power generated void disturbances which are caused by rod oscillation.

f. Steady-state flux noise recorded on in-core ion chambers varies in frequency content with position in the reactor. Ion chambers one-fourth of the way up from the bottom of the core and the external ion chambers both have very little high frequency noise (3 - 30 cps). In the high flow center region of the core, ion chambers located higher up in the core showed increasing high frequency content. In the outer, flow orificed regions of the core, very little high frequency flux noise was present. Core voids were very high and velocities very low in this region.

g. Recirculation pump system noise was shown not to have a defined influence upon core responses.

4. Conclusions

The VBWR stability experiments have produced detailed information regarding in-core fluxes and flows as well as system operational parameters. These have been assembled from known measurement techniques and analytical methods into what appears at this point to be a comprehensible and understandable picture of the stability, transient response, and operational noise character of the reactor and system. The conclusions are based upon experimental points taken over a range which was indicated to best demonstrate the responses of the reactor.

a. Absolute Stability

Although the pre-test analysis parametric studies were not always done at conditions as close as desired to test conditions to produce refined relationships, the following may be stated:

(1) The reactor stability theory described in GEAP-3971 predicts the stability characteristics of the VBWR well for natural circulation operation of the plant. Forced circulation operation conditions are predicted equally well for systems whose flow velocities in the two-phase region are not too far removed from natural circulation. It is believed that this theory is adequate for any boiling water reactor having similar characteristics to the VBWR.

(2) High flow rate (for instance above 4 - 5 fps inlet velocity) forced circulation plants will require additional work on the theory.

(3) The two most significant parameters affecting the absolute stability of this reactor are:

(a) The void coefficient of reactivity.

(b) The condition of system hydraulics.

The VBWR, as it was operated during these tests, showed a greater sensitivity to the void coefficient of reactivity. It is concluded that these two parameters would be the first two which affect the VBWR stability. Other parameters, such as pressure and fuel time responses, can have sizeable effects in some reactor systems.

(4) Determination of the average parameter or average channel responses needs further work to establish a close relationship between predicted and test performance. Spatial representations of thermal hydraulics and void reactivity coefficients are key investigations in this area.

(5) Rules of thumb for predicting absolute stability are of little use in high flow, forced circulation systems. A system analysis, as described in GEAP-3971, is much more reliable than intuitive treatment.

(6) It is concluded that operational noise cannot be used as a measure of absolute stability. This conclusion is discussed more fully in the operational noise conclusions.

(7) Rod oscillation tests have provided significant and quantitative absolute stability data in these tests; steady-state noise and transient response tests have not. Rod oscillator tests should be conducted on every boiling water reactor which has significant design differences from those for which there is absolute stability data.

(8) Quantitative data, derived from hydraulic stability loop tests, are required for void transfer functions. These important data will provide a basis for model analysis improvement in the thermal hydraulic response area, and in the average parameter analysis area.

(9) An advanced analysis program is required to obtain really significant gains from the work conducted thus far. Such a program is outlined in GEAP-3971.

b. Operational Noise and Its Effect on BWR Stability

(1) The VBWR experiments definitely show that steady-state oscillations in power or flow cannot be used as an indication of absolute BWR stability. These tests, in fact, show flux and flow parameters which indicate the wrong direction in stability trends. A reactor operator, it is concluded, would need specific knowledge of:

(a) Reactor system characteristics,

(b) Sources of reactor excitation, and

(c) Frequency and magnitude distribution of noise excitations,

to make satisfactory conclusions.

(2) It is concluded that orificing of flow channels produces a considerable reduction in noise amplitude.

(3) The VBWR test data and the accompanying hydraulic stability loop test program give promise of significantly improved understanding of noise phenomena in boiling water reactors. Two aspects are worthy of note:

(a) The natural circulation rod oscillator tests are a source of in-core information on core and flow responses to specific excitations, namely, the rod oscillation.

(b) A theory has been advanced for propagation of disturbances from excitation forces. The theory predicts the correct range of frequencies for the measured responses of VBWR.

No definite conclusions will be drawn for these items except to say that they are plausible contributions to explain portions of the measured phenomena and provide a good basis for initial detailed work on noise.

HYDRAULIC STABILITY LOOP

The test loop which is described in GEAP-3935[18] was operated in natural circulation to examine steady-state, power impulse, and power oscillation responses of various parameters, but primarily flow. Steady-state and transient results were reported in GEAP-4215 and GEAP-4159.[19, 20] Some significant understanding of the analytical model was obtained from these runs.

The steady-state responses of flow were shown to be predicted very well by the stability and transient response code. A maximum error of 8 percent in flow at 3 percent steam quality was found. This accuracy of calculation is very good for two-phase flow systems. This conclusion applies to natural circulation operation. No forced circulation tests were conducted under the Fuel Cycle Program.

Power impulse tests were conducted to demonstrate the oscillatory characteristics of two-phase flow and to make qualitative observations about the analytical model. The following information was obtained from a power impulse transient test:

1. Damped oscillation frequency
2. Quadratic damping coefficient
3. Time lags (or phase) of pressure and velocity to power impulse. Information on pressure propagation.
4. Magnitude and character of pressure and velocity changes.

The following conclusions were reached about two-phase flow transients in channels:

1. Undamped and (self-excited) oscillatory responses are easily obtained by parametric changes and small disturbances.

2. The pressure in the heater rises in response to power oscillations without a change in pressure difference across the channel. The heater fluid acts as a capacitance under these circumstances. This effect seems to be the most energetic effect which presents itself. It seems likely to provide an explanation for some major portion of the discrepancies between VBWR test and the theory.

3. Intermediate subcooling operation showed flow responses were less stable than higher or lower subcooling runs.

4. The frequency dependent theory is not, at present, in a form well-suited to prediction of transients.

Power oscillation tests with natural circulation were conducted during May and June 1963, but not analyzed under Fuel Cycle funding. The data analysis and comparison of experiment and theory are presented here to provide a quantitatively complete representation of the stability and transient response theory. The parametric variation of four runs studied in detail are shown in the following tabulation.

NATURAL CIRCULATION

	SATR Run No. 5-31-01-002	Loop Run No. 5-31-01
V	4.35 fps	4.25 fps
H_s	42.9	42.7
X	10.4 percent	11.9 percent
Resistance Type - Minimum		(Flowmeter of unusually high flow resistance)

NATURAL CIRCULATION (Continued)

SATR		Loop
SATR Run No. 5-24-01-001		Loop Run No. 5-24-01-c
V	4.33 fps	4.24 fps
H_s	14.9	14.7
X	7.0 percent	7.1 percent
Resistance Type - Minimum		(Flowmeter of unusually high flow resistance)
SATR Run No. 5-28-01-002		Loop Run No. 5-28-01
V	4.2 fps	4.13 fps
H_s	32.8	32.8
X	14.9 percent	14.9 percent
Resistance - Minimum		(Flowmeter of unusually high flow resistance)
SATR Run No. 5-27-01-001		Loop Run No. 5-27-01
V	3.49 fps	3.61 fps
H_s	16.8	16.8
X	20.8 percent	21.5 percent
Resistance - Minimum		(Flowmeter of unusually high flow resistance)

The four tests present a preliminary indication of the stability and transient response code responses to power oscillation compared to test data. In order to demonstrate the expected variation of velocity responses to subcooling changes, Run 5-28-01 is recalculated for 40 percent change in subcooling. This gives an evaluation of the magnitude of velocity response. Figure 15 shows this sizeable change in velocity response.

Figures 16 through 22 show magnitude and phase plots of the four tabulated runs. Power oscillation runs were discussed in GEAP-4301.[21] The following observations should be made of these figures.

1. Magnitude curves of $\frac{V^*}{Q^*}$, the velocity response to a power oscillation, follow the amplitude of the harmonics of the flow disturbance surprisingly well, indicating the character of the theoretical response to be correct.

2. Most phase-lag curves demonstrate a drift of high frequencies to a greater phase lag than predicted by theory.

3. The high-quality (20 percent), intermediate subcooling (16.8 Btu) run 5-27 shows the best correspondence with theory of the four cases.

4. Frequencies of the fundamental appear quite accurately determined in all cases.

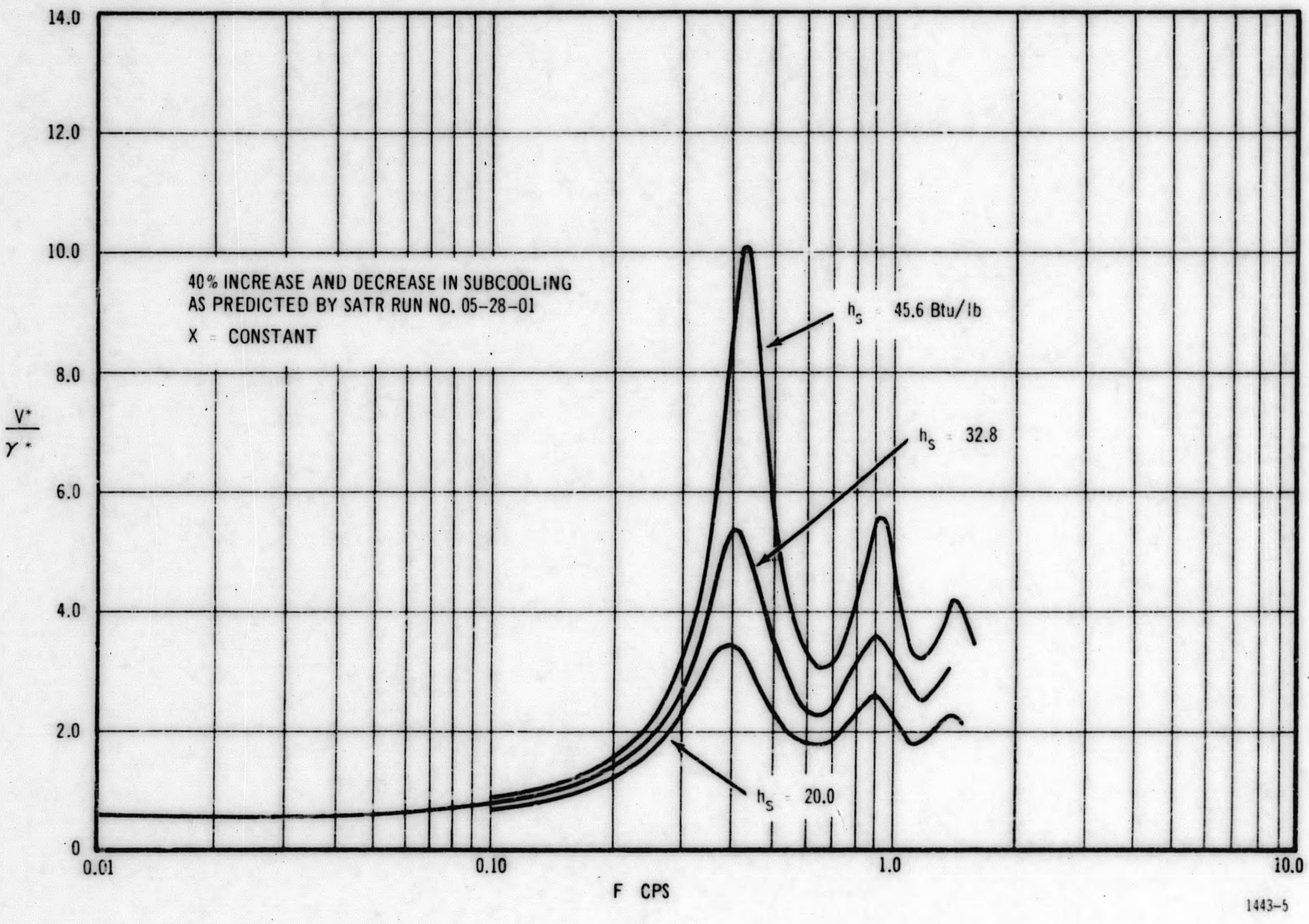

Figure 15. Calculated Effect of Subcooling on Velocity Response

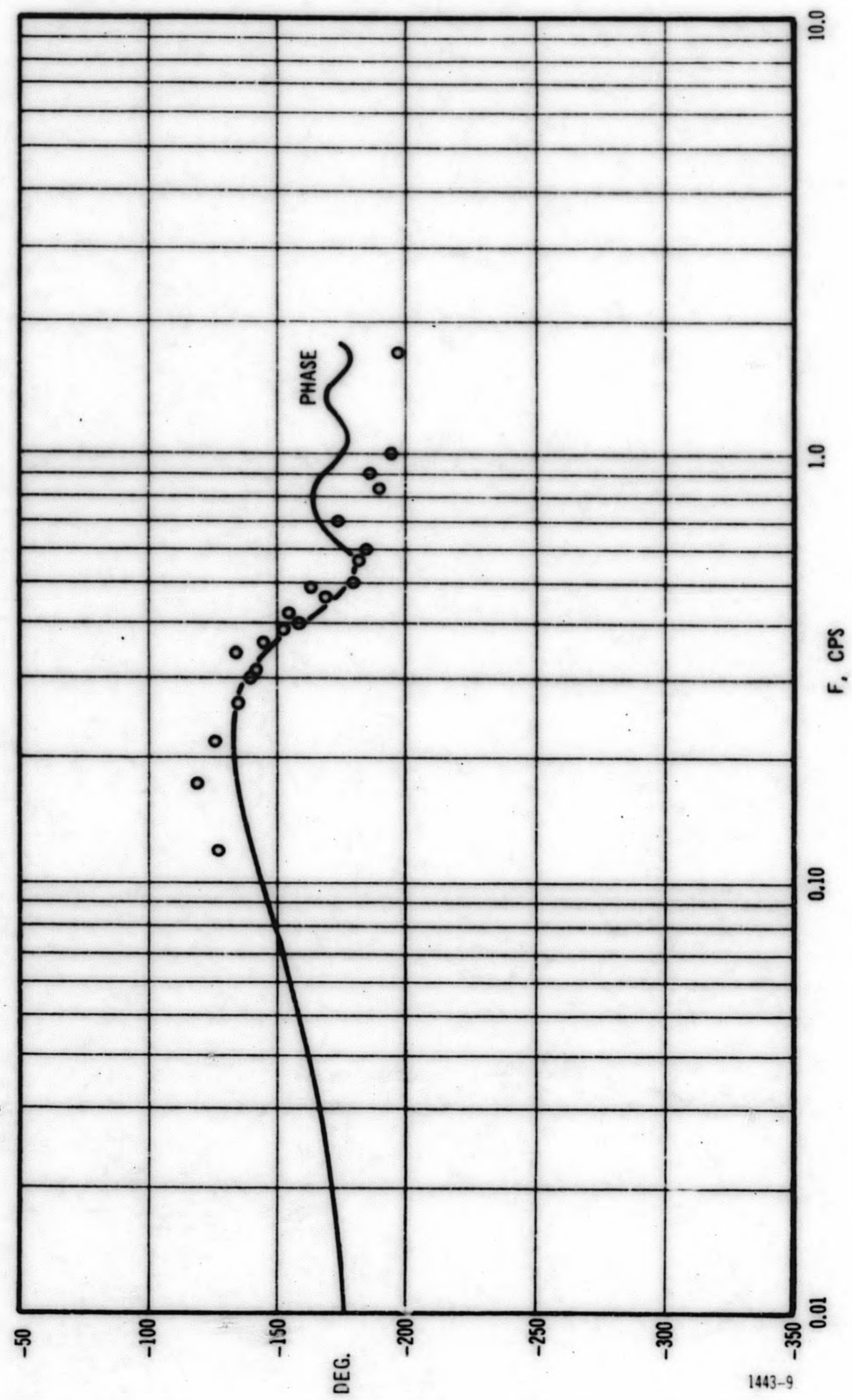

Figure 16. Velocity Response, Run 5-27-01

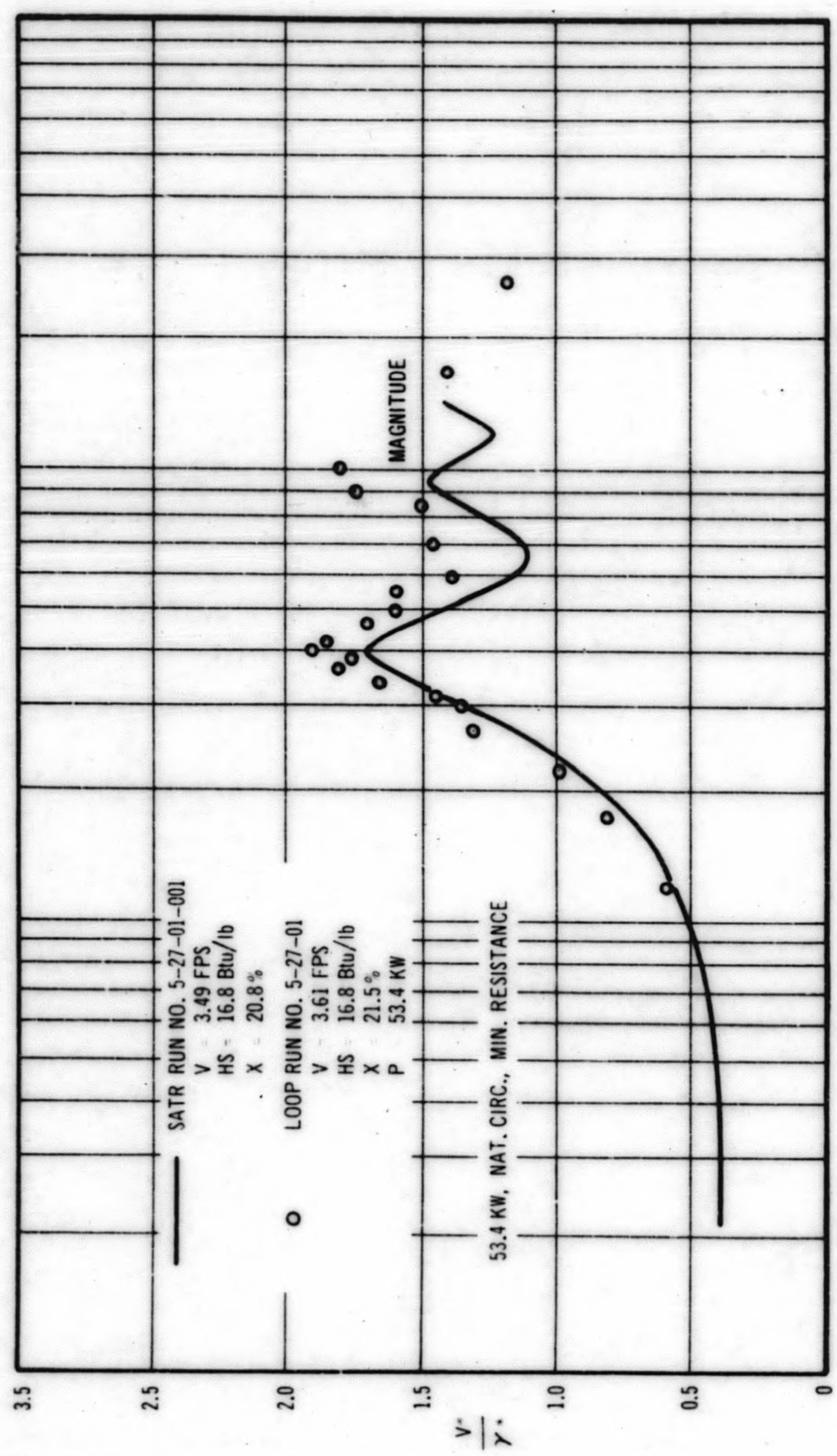

Figure 17. Velocity Response, Run 5-27-01

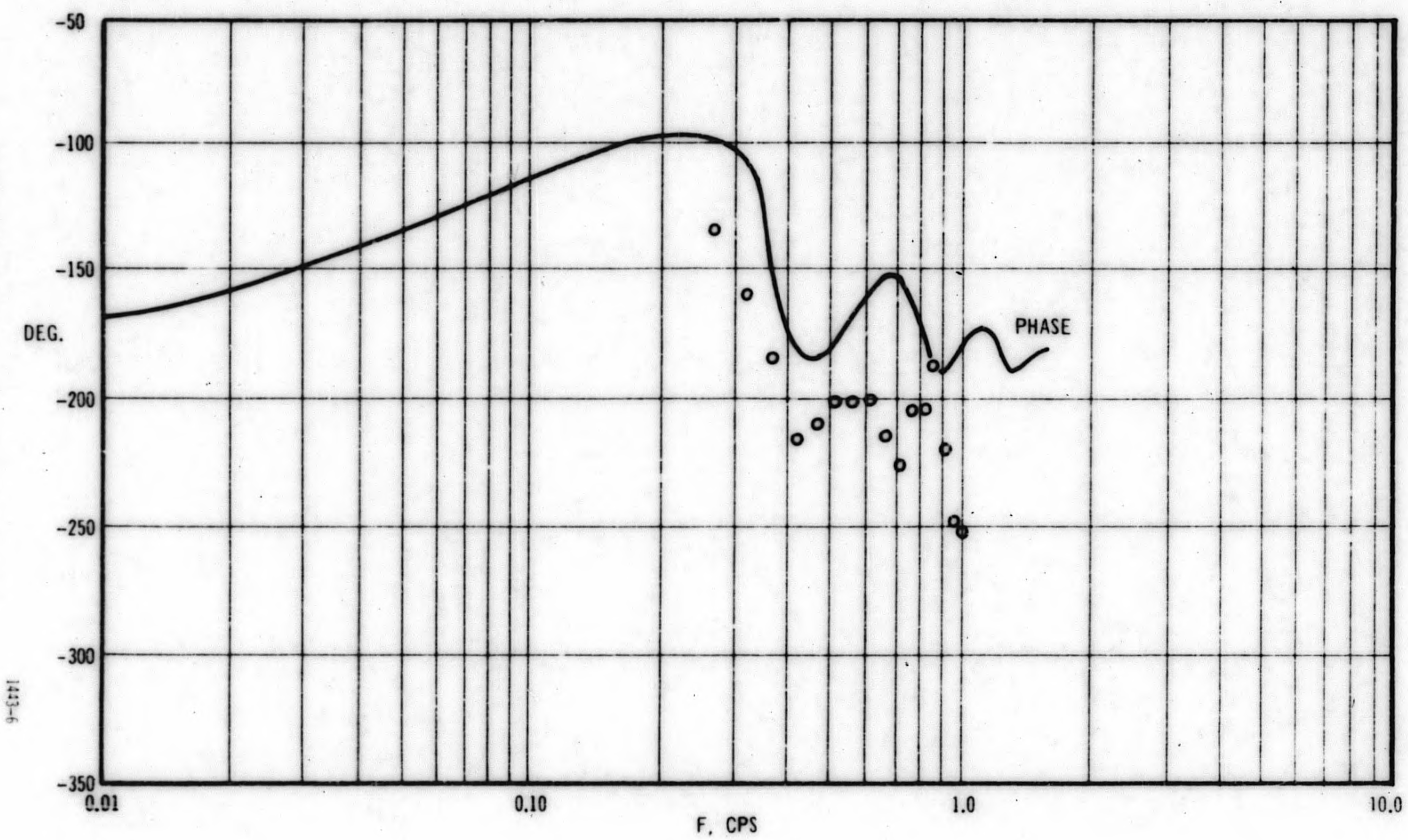

Figure 18. Velocity Response, Run 5-31-01

1443-6

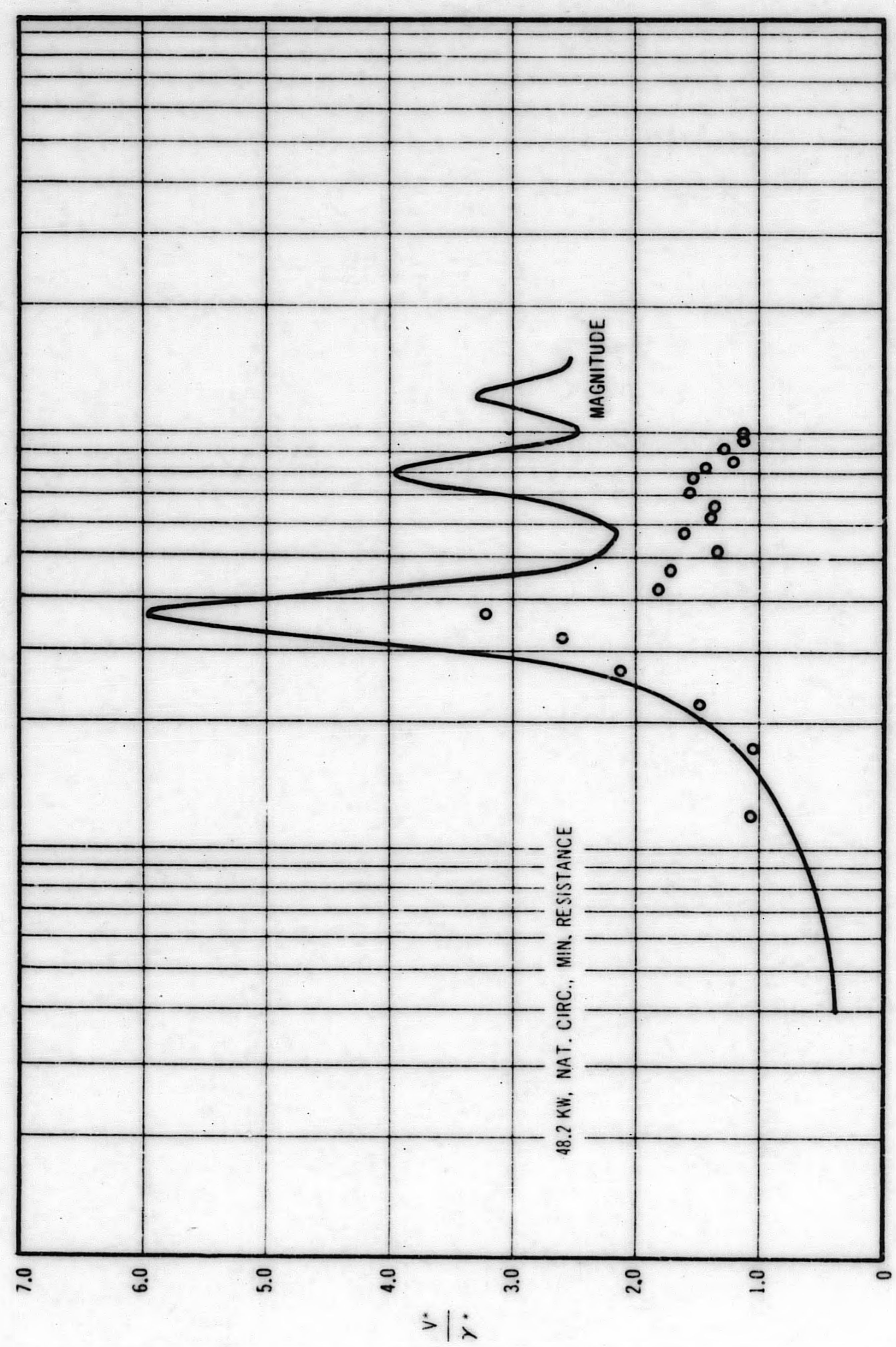

Figure 19. Velocity Response, Run 5-31-01

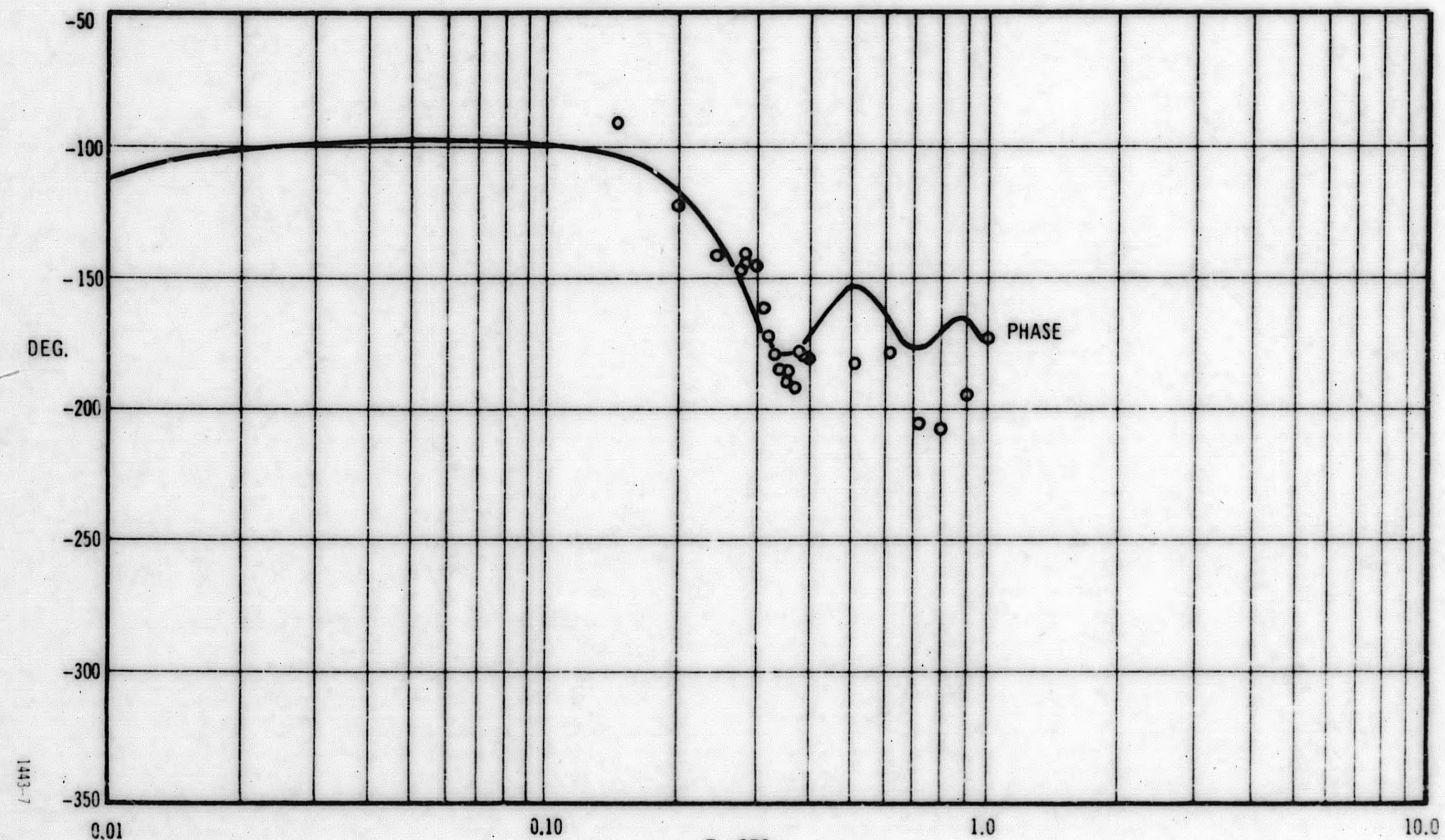

Figure 20. Velocity Response, Run 5-24-01

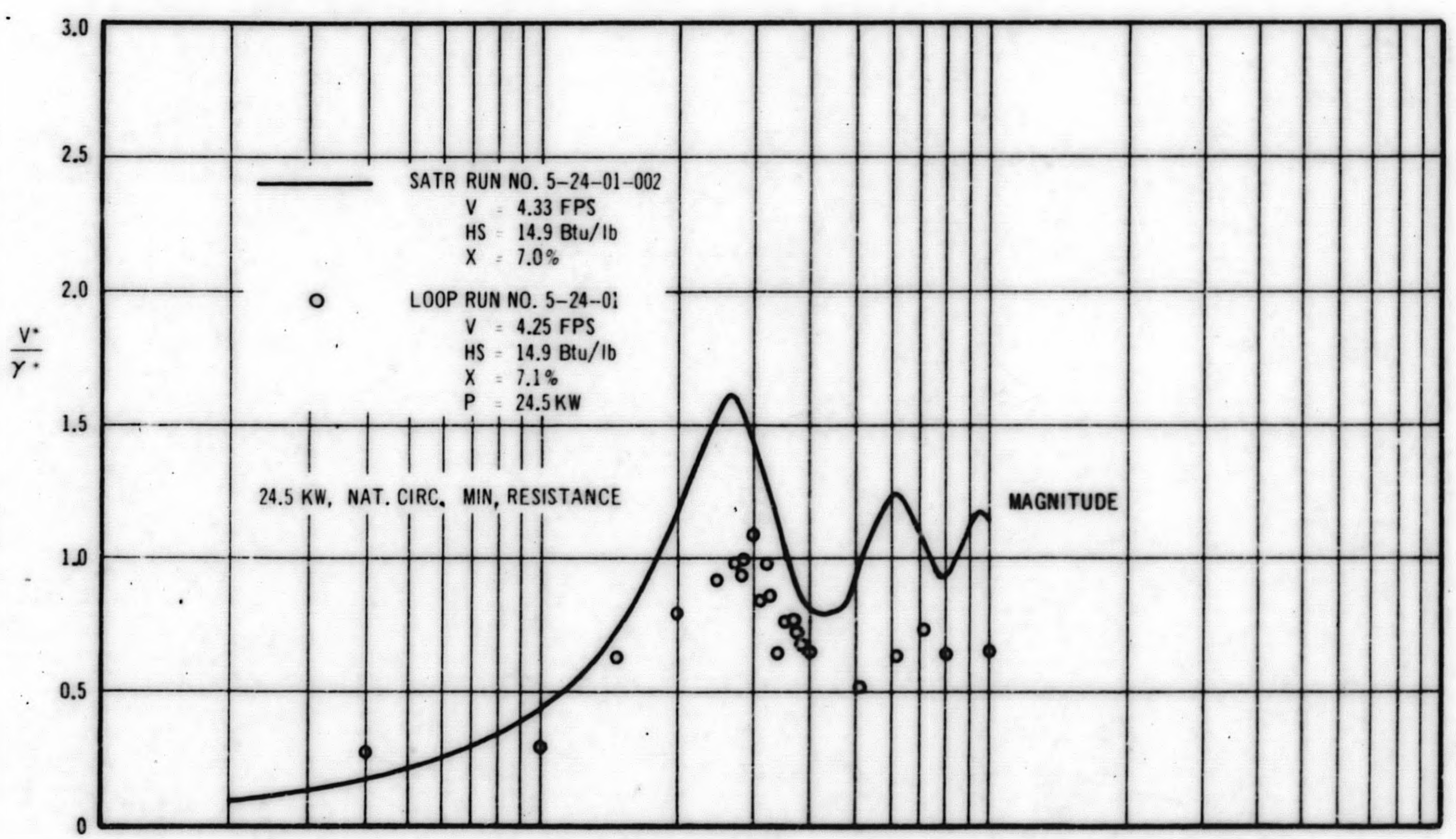

$\frac{V^*}{\gamma^*}$

Figure 21. Velocity Response, Run 5-24-01

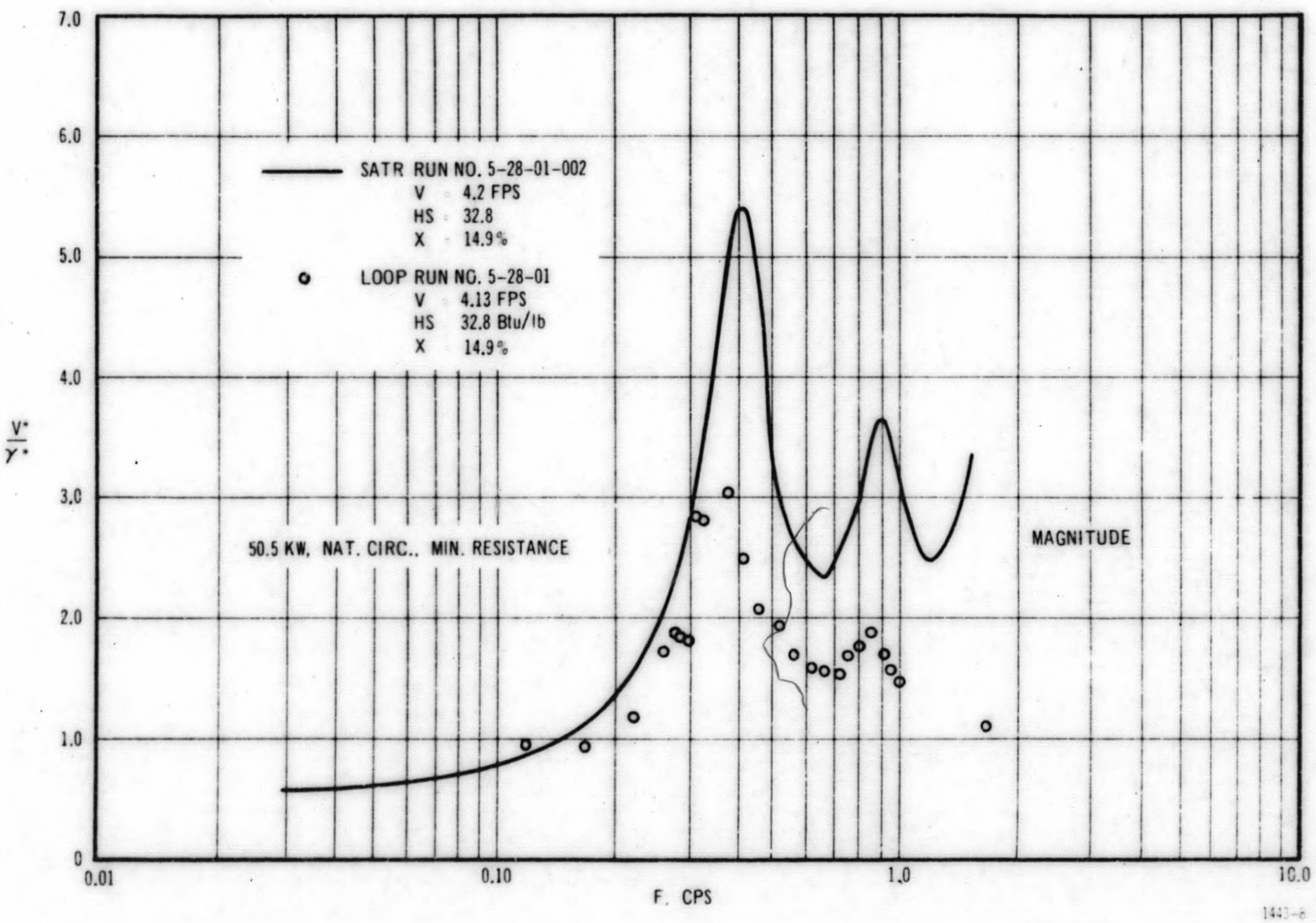

Figure 22. Velocity Response, Run 5-28-01

GFAP-4481

5. Lower quality runs appear to produce lower magnitude oscillations and larger phase lags than the theory predicts.

6. Experimentally, it was determined that there was a greater single-phase loss than was used in the theoretical calculations. This was due to greater loss in the turbine flow-meter than was expected.

NOISE

GEAP-3971 expresses a number of conclusions regarding flux noise in the VBWR. They have been outlined in the above discussion of that report. The most forceful conclusion reached is that steady-state noise observation does not give an indication of stability of a BWR.

GEAP-4301[21] provides an accurately determined VBWR noise spectrum derived using the DART code. Figure 23 shows this spectrum. The significant result is that noise components above 1 cps are of insignificant influence in VBWR fluxes. The proposed contributors to noise have been:

1. Operational transients
2. Surface distrubances (GEAP-4061)[22]
3. Propagation of disturbances in time and space (GEAP-4094)[23]
4. Two-phase bubble dynamics (GEAP-3971)

Since quantitative frequencies have been obtained in items (2) and (3), theoretically these may be compared to VBWR noise. Item (3), disturbance propagation, predicted a range of frequencies from 0.7 to 10 cps originating in the region of the core. Item (2), the surface distrubance, calculates frequencies of 0.6 to 3 cps. These are disturbance frequencies propagated to the core. Examining Figure 23, most of these frequencies do not appear of sufficient magnitude to be significant in the VBWR. GEAP-4301[21] considered also the driving function spectrum for noise, and showed it to be very non-white and composed primarily of low frequencies. This tends to support operational transients as the cause.

An improved understanding of factors entering into noise has been obtained from the following:

1. A calculation of the minimum energy needed to excite the in-channel flows.
2. An air water experiment to observe the propagation of pressure disturbances in two-phase media.

Examination of flow traces of channels for rod oscillation tests with the VBWR operating in natural circulation shows that the flow is ordered, but that its amplitude has not been changed. This energy input was shown to produce at least 12 times the response that the maximum surface disturbance could produce if it were all transmitted to the core inlet. GEAP-3971 provides details of this.

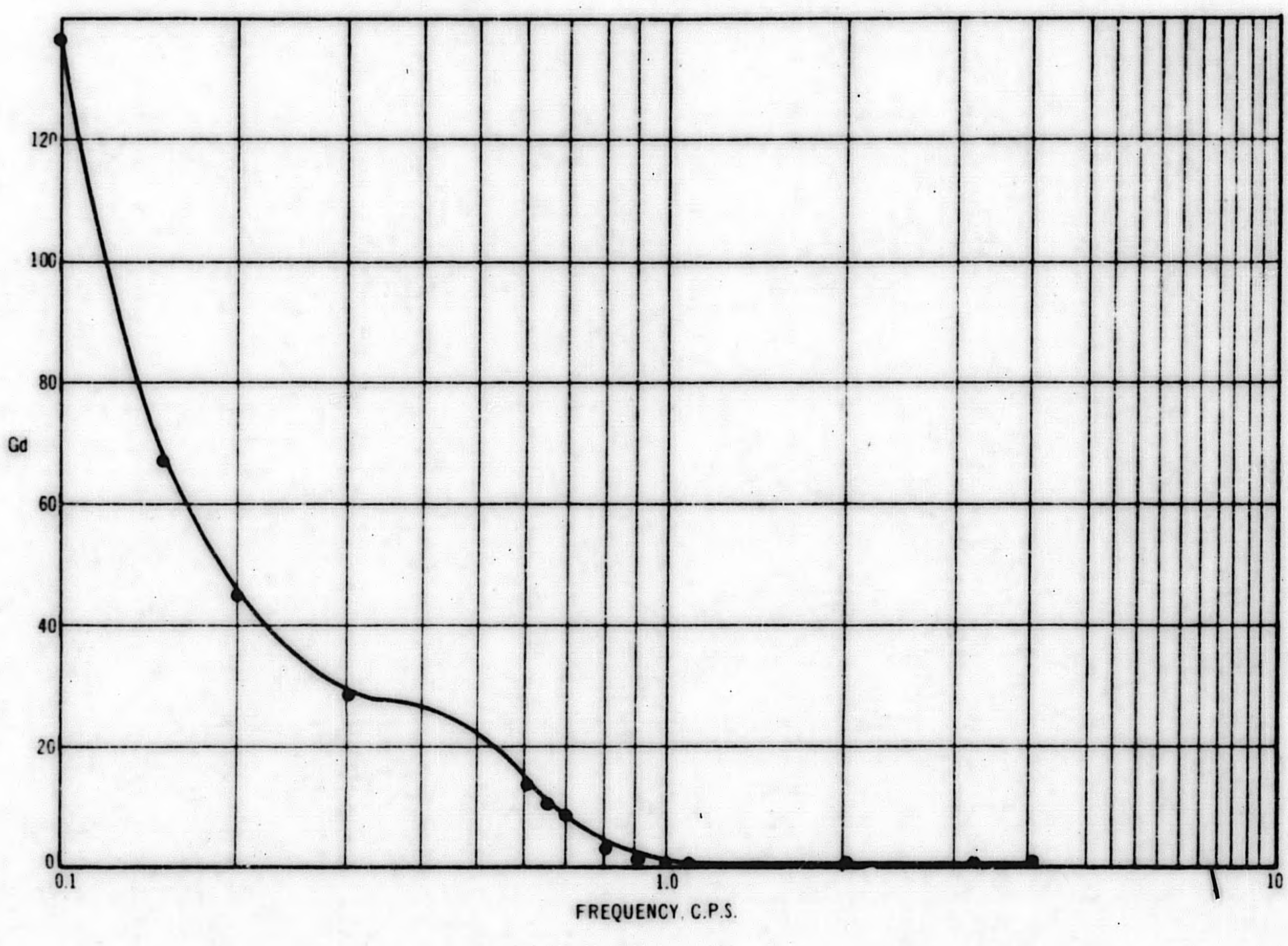

Figure 23. Reactivity Driving Spectra vs. Frequency

Figure 24 shows air-water test measurements which were made below the surface of the liquid in the vessel, and in the two-phase flow region of a mockup natural circulation system which had been scaled to VBWR dimensions. The tests were described in GEAP-4159.[20] Pressure peaks resulting from resonant disturbances are shown in both cases.

If the resonant peak heights are considered in the range of interest (0 - 2 cps), the maximum transmission of a pressure peak to the bottom of the two-phase zone (3 feet distant) is 5 to 6 percent when the background noise is removed.

This means that a smaller quantity would be transmitted in greater distance. Transmission properties of atmospheric and 1000 psia are indicated by Karplus (reference 24) to be about the same.

This means that disturbances which show up as noise in a reactor must be generated in a vicinity of the measurement; or must be the working in unison of a group of local disturbances; or, lastly, must be systematically derived, that is, a result of system parameter changes.

Thus, if the static pressure were raised, its effect would be felt by the core, but if a pressure wave were traveling through the medium without a net change of pressure, its effect would be greatly diminished.

Thus far, core local disturbances have been associated primarily with high frequencies. Systematic disturbances are characteristically lower frequencies.

DATA ANALYSIS

Resolution of a mathematically accurate data analysis method is a major step in understanding stability and transient response of a reactor system. The initial tools available at the time the Fuel Cycle Development Program was initiated were very limited, and suspected of sizeable errors. The analytical equipment which was used to analyze the VBWR stability test results, for example, was a bandpass filter circuit described in GEAP-3971. This equipment was expected to produce good results for rod oscillation tests having large periodic signals, but poor results for steady-state noise analysis.

Attempts were made to obtain a digital auto correlation code (AUTO) as described in GEAP-3971 and GEAP-4094.[23] This code was found to give physically unrealistic results. A subsequent code, DART, was developed by APED and described in GEAP-4301.[21] This development has produced the theoretically and physically expected results. Such a code is very accurate but also expensive and difficult to use.

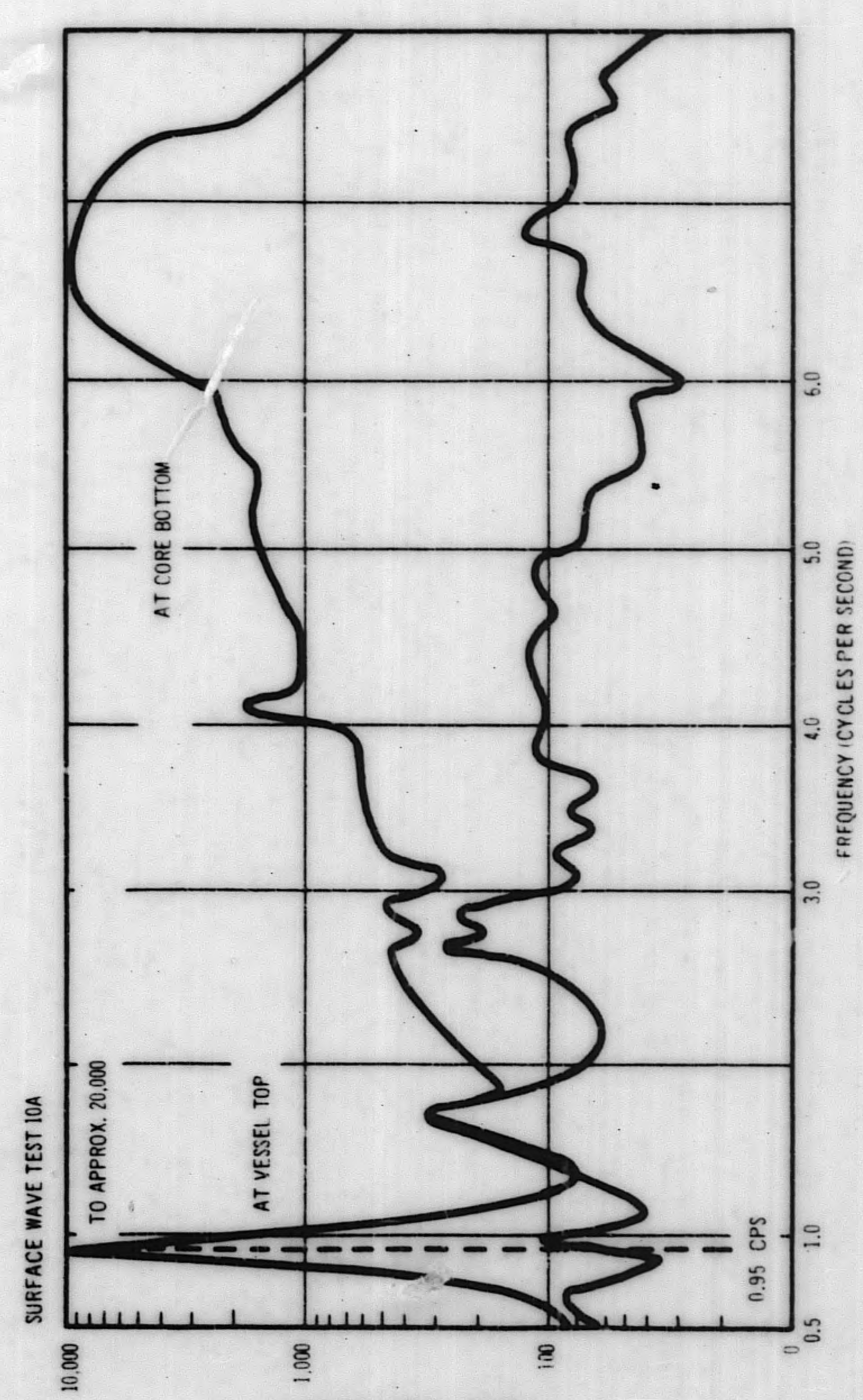

Figure 24. Spectral Power Intensity vs Frequency

Analysis of the mathematics of spectrum analysis indicated that an analog Fourier spectrum analyzer could be built to perform the same operations as the DART code. A commercially available analyzer built by the Boonshaft-Fuchs Company was obtained and its accuracy checked against the DART code. The Fourier spectrum analyzer produces comparable results to those of the DART code. Significant improvements have been seen in the spectra obtained for rod oscillation tests of the VBWR.

NOMENCLATURE

$N*$	Normalized neutron flux
h	Enthalpy
ΔK	ΔReactivity - dollars
P	Pressure - psi
x	Vertical height in channel
R	Local voids at (x)
u	Core voids (average), U* normalized core voids
s	Steam velocity
W	Two-phase water velocity
v .	Inlet water velocity
L	Boiling length
G_w	Water-wall shear term
G_{ws}	Steam-water shear term
g	Acceleration of gravity
t	Time
$q(x, t)$	Local heat input
Q^*	Normalized heat input
τ_c	Transit time for the void sweep
ρ_w	Density of water
ρ_s	Density of steam
γ	$Q/A \rho_w (h_s - L_w)$ Power parameter
β	ρ_w/ρ_s Density parameter
α	$\frac{h_w - h_{sc}}{h_s - h_w}$ Subcooling parameter
Γ_w	Shear stress - water and wall
Γ_{ws}	Shear stress - Steam and water

REFERENCES

1. Hodde, J. A., " Fuel Cycle Program - A Boiling Water Reactor Research and Development Program - Eighth Quarterly Progress Report," GEAP-4048, April - June, 1962.

2. "High Power Density Development Project - Thirteenth Quarterly Progress Report," GEAP-4309, April - June, 1963, July, 1963.

3. "High Power Density Development Project - Ninth Quarterly Progress Report, GEAP-4049, April - June, 1962, July, 1962.

4. "High Power Density Development Project - Tenth Quarterly Progress Report," GEAP-4096, July - September, 1962, October, 1962.

5. "High Power Density Development Project - Eleventh Quarterly Progress Report," GEAP-4155, October - December, 1962, January, 1963.

6. "High Power Density Development Project - Twelfth Quarterly Progress Report," GEAP-4219, January - March, 1963, April, 1963.

7. "High Power Density Development Project - Fourteenth Quarterly Progress Report," GEAP-4391, July - September, 1963, October, 1963.

8. Fowler, W. D., Lingafelter, J. W., "Design and Fabrication of High Power Density Fuel Assemblies from VBWR Irradiation Testing," GEAP-3609, November, 1960.

9. Baroch, C. J., Hoffmann, J. P., Rous, W. C., "AEC Fuel Cycle Program - Design and Fabrication of the Basic Fuel Assemblies," GEAP-3653, March, 1963.

10. deHalas, D., Horn, G. R., "Evolution of Uranium Dioxide Structure During Irradiation of Fuel Rods," HW-SA-2650, June, 1962.

11. Hoffmann, J. P., "Design and Fabrication of Fuel Rods for High Thermal Performance Life Demonstration, Results of Centermelt Calibration Test," AEC Fuel Cycle Program, GEAP-4406, to be published.

12. "Eighth Quarterly Progress Report, EURAEC High Performance UO_2 Program," GEAP-3771-8, April 15, 1963.

13. Cook, W. H., et al., "Plan for VBWR Stability Experiment," GEAP-3794, August 30, 1961.

REFERENCES (Continued)

14. "Third Quarterly Report - Fuel Cycle Development Program," GEAP-3709, January - March, 1961.

15. Case, J., Holland, L. K., "Consumers Big Rock Nuclear Power Reactor Stability Analysis," GEAP-3975.

16. Case, J. M., "Neutron and Parallel Flow Channel Coupling Effects in the T-7 Flux Trap Reactor," GEAP-3508, August 15, 1960.

17. Holland, L. K., Harriman, J., "Heat Transfer from a Cylindrical Rod with Internal Heat Generation," GEAP-0805, November. 14, 1955.

18. Hodde, J. A., "Fuel Cycle Program - A Boiling Water Reactor Research and Development Program - Seventh Quarterly Progress Report," GEAP-3935, January - March, 1962.

19. Howard, C. L., "Fuel Cycle Program - A Boiling Water Reactor Research and Development Program - Eleventh Quarterly Progress Report," GEAP-4215, January - March, 1963.

20. Howard, C. L., "Fuel Cycle Program - A boiling Water Reactor Research and Development Program - Tenth Quarterly Progress Report," GEAP-4159, January 14, 1963.

21. Howard, L. C., "Fuel Cycle Program - A Boiling Water Reactor Research and Development Program, Twelfth Quarterly Progress Report," GEAP-4301, April - June, 1963.

22. Howard, C. L., Hamilton, R. G., "Water Surface Waves in Boiling Water Reactors," GEAP-4061, August 31, 1962.

23. Howard, C. L., "Fuel Cycle Program - A Boiling Water Reactor Research and Development Program - Ninth Quarterly Progress Report," GEAP-4094, July - September, 1962.

24. Karplus, H. B., "Propagation of Pressure Waves in a Mixture of Steam and Water," ARF-4132-12, January, 1961.

ACKNOWLEDGMENT

The Fuel Cycle Program is sponsored by the AEC and is conducted by the General Electric Company with the following individuals contributing to the program during the quarter:

Project Engineer	C. L. Howard
Project Consultant	S. Levy
Fuel Development	T. J. Pashos
	H. E. Williamson
	C. J. Baroch
	J. P. Hoffmann
	F. H. Megerth
	S. Y. Ogawa
	J. A. Whittington
Stability	W. H. Cook
VBWR Core Analysis	J. O. Arterburn
	R. A. Becker
	T. Tillinghast
VBWR Programming	H. D. Ongman
VBWR Operation	J. B. Violette
Test Program Engineering	E. L. Burley
	R. H. Silletto
	VBWR Staff
Vallecitos Radioactive Material Laboratory	R. F. Boyle

Approved by:

C. L. Howard

C. L. Howard, Project Engineer
Fuel Cycle Development Program

D H Imhoff

D. H. Imhoff, Manager
Engineering Development

ATOMIC POWER EQUIPMENT DEPARTMENT
GENERAL ELECTRIC
SAN JOSE, CALIFORNIA

END